Memory burden effect in black holes and solitons: Implications for PBH

Gia Dvali,[1,2] Juan Sebastián Valbuena-Bermúdez,[3,*] and Michael Zantedeschi[4,5,†]
[1]*Arnold Sommerfeld Center, Ludwig-Maximilians-Universität, Theresienstraße 37, 80333 München, Germany*
[2]*Max-Planck-Institut für Physik, Boltzmannstrasse 8, 85748 Garching, Germany*
[3]*Institut de Física d'Altes Energies (IFAE) and The Barcelona Institute of Science and Technology (BIST), Campus UAB, 08193 Bellaterra (Barcelona), Spain*
[4]*Tsung-Dao Lee Institute (TDLI), No. 1 Lisuo Road, 201210 Shanghai, China*
[5]*School of Physics and Astronomy, Shanghai Jiao Tong University, Dongchuan Road 800, 200240 Shanghai, China*

(Received 14 June 2024; accepted 22 August 2024; published 13 September 2024)

The essence of the memory burden effect is that a load of information carried by a system stabilizes it. This universal effect is especially prominent in systems with a high capacity of information storage, such as black holes and other objects with maximal microstate degeneracy, the entities universally referred to as "saturons." The phenomenon has several implications. The memory burden effect suppresses a further decay of a black hole, the latest, after it has emitted about half of its initial mass. As a consequence, the light primordial black holes that previously were assumed to be fully evaporated are expected to be present as viable dark matter candidates. In the present paper, we deepen the understanding of the memory burden effect. We first identify various memory burden regimes in generic Hamiltonian systems and then establish a precise correspondence in solitons and in black holes. We make transparent, at a microscopic level, the fundamental differences between the stabilization by a quantum memory burden versus the stabilization by a long-range classical hair due to a spin or an electric charge. We identify certain new features of potential observational interest, such as the model-independent spread of the stabilized masses of initially degenerate primordial black holes.

DOI: 10.1103/PhysRevD.110.056029

I. INTRODUCTION

The phenomenon of memory burden, originally described in [1], is summarized in the following statement: Information loaded in a system resists its decay.

Naturally, the effect is especially sound in systems with enhanced information storage capacity. This capacity can be quantified by the number and degeneracy of microstates that the system possesses for the given values of macroscopic parameters, such as, e.g., the radius R and the total energy.

Black holes are the prominent representatives of this category. This is obvious from Bekenstein-Hawking entropy [2],

$$S_{\rm BH} = \pi R^2 M_{\rm P}^2, \tag{1}$$

where $M_{\rm P}$ is the Planck mass. Correspondingly, it was suggested in [1,3] that the phenomenon of memory burden must be applicable to black holes.

This effect explains, in terms of an explicit microscopic mechanism, why, at the early stages of Hawking's decay, the information stored in a black hole cannot be released together with radiation. This matches the semiclassical expectation.

However, an important new feature emerges. The internally maintained information backreacts and creates resistance against the decay of a black hole. This is the effect of the memory burden phenomenon in a black hole.

Furthermore, by performing a detailed analysis of the prototype systems, it was concluded in [3] that not only do black holes undergo the memory burden effect, but they likely are stabilized by it. That is, in the process of a black hole decay, the memory burden grows, and after a certain characteristic time, $t_{\rm M}$, reaches a critical value. $t_{\rm M}$ is bounded from above by the age of a black hole that lost about half of its initial mass.

At this point, the black hole has evolved into a "remnant" that cannot continue an ordinary quantum decay. A remarkable feature is that the remnant is macroscopic, with a mass comparable to the initial black hole. The fate of

*Contact author: jvalbuena@ifae.es
†Contact author: zantedeschim@sjtu.edu.cn

this object cannot be determined by applying a standard semiclassical analysis that would be valid for a young black hole.

As pointed out in [3], at the current level of understanding, it is not excluded that some new collective (classical) instability sets in, leading to a disintegration of the memory-burdened remnant.

Putting this possibility aside, after a black hole enters the memory burden phase, its evaporation must slow down dramatically. From the analyticity considerations, it was suggested in [3] that the remaining lifetime of a black hole scales as

$$\tau \sim R S_{\rm BH}^{1+k}, \tag{2}$$

where $S_{\rm BH}$ is the entropy of initial black hole and $k > 0$ is an integer.

This has a number of implications which will be discussed later, after we introduce the second part of the story.

On the other hand, it was shown recently [4–6] that black holes are not the only objects with maximal information storage capacity. Rather, in various consistent quantum field theories (QFTs) there exist a whole class of objects, named "saturons" [4], that exhibit the identical properties.

An important aspect is that saturons can emerge in the form of solitons and other bound states in renormalizable QFTs at weak coupling where their properties are fully under control and calculable [4–12].

In order to fix the definition: a saturon represents an object that saturates the QFT upper bound on the microstate degeneracy. The bound has been formulated in [4] and can be given in two equivalent forms as the bound on the microstate entropy, $S \equiv \ln(n_{\rm st})$, with $n_{\rm st}$ number of degenerate microstates.

First, for a bound state of radius R formed by QFT degrees of freedom interacting via a running coupling α, the upper bound on the microstate entropy is

$$S \leq \frac{1}{\alpha}, \tag{3}$$

where α must be evaluated at the scale $1/R$.

Equivalently, the bound can be written in terms of the Goldstone scale, f, of the spontaneously broken Poincare symmetry:

$$S \leq \pi R^2 f^2. \tag{4}$$

As shown in [4], the above bounds set the maximal degeneracy reachable within the validity of the QFT description. In particular, their saturation is correlated with the saturation of unitarity by the scattering amplitudes.

As already discussed in [4], Bekenstein-Hawking entropy of a black hole (1) represents a particular case of saturation of both bounds. First, applied to a black hole, the formula (4) is identical to (1), since for a black hole of arbitrary mass, the scale of Poincare Goldstone is given by the Planck mass, $f = M_{\rm P}$.

Simultaneously, the black hole entropy (1) is also equal to (3), since the gravitational coupling, evaluated at energy scale $1/R$, is $\alpha_{\rm gr} = 1/(\pi R^2 M_{\rm P}^2)$.

It has been observed that striking similarities between black holes and saturons of renormalizable QFTs extend to their other key properties:

(1) Impossibility of the information-retrieval classically [4–7,9,10].
(2) The minimal timescale of the start of the information-retrieval, $t \sim S\ R$, which is identical to the Page's time in black holes [4,9,10].
(3) The existence of information horizon in the semiclassical theory [10].
(4) Thermal-like evaporation at initial stages of the decay [9,10].
(5) The relation between the maximal spin and the entropy [11,12].

The above correspondence makes the study of saturons important due to the following reasons. First, it shows that the black hole properties are not specific to gravity and can be understood within calculability domains of renormalizable QFTs.

Second, saturons can serve as laboratories for understanding the microscopic nature of known black hole properties and for discovering new features.

In the present paper, we shall apply this strategy to the memory burden effect in two directions. First, following [1,3], we outline the generic properties of the memory burden phenomenon within Hamiltonian models of enhanced information capacity. We then demonstrate the concrete manifestations of these properties within solitons, expanding the earlier analysis of [10,13]. Next, we establish the link with analogous properties in black holes.

In studying the memory burden effect in black holes, we shall use two strategies. On one hand, we shall extract the key features of the effect relying solely on the universality of the phenomenon and the requirement of QFT consistency of the system.

On the other hand, we shall cross-check our conclusions with a microscopic theory of black hole's quantum N portrait [14–16]. In this picture a black hole is described as a saturated coherent state of gravitons at criticality, which makes the origin of its enhanced information storage capacity very explicit.

This approach allows us to predict certain new features of memory burden in black holes, moving forward from the previous studies.

The memory burden effect has a wide range of applications. As already put forward in [3], one immediate application is the opening up of a new window of the primordial black hole dark matter with masses below 10^{14} g. In the standard treatment, this interval of masses was

ignored based on the assumption of the validity of the semiclassical picture during the black hole's entire lifetime. The memory burden effect invalidates this assumption.

Some viable examples of PBH dark matter in the new mass window were given already in [3]. Further studies, focusing on the formation mechanisms [17] and various constraints on memory burdened PBH dark matter [18–21], have also been performed.

In the present paper, we shall predict a new feature of potential observational significance: the model-independent spread in PBH masses induced by the memory burden effect.

As suggested in [22], another entity, likely subjected to the memory burden effect, is a de Sitter Hubble patch of radius R. Similarly to a black hole, de Sitter carries a maximal microstate entropy of Gibbons-Hawking [23] given by the expression (1). Due to this, it falls in the category of systems with enhanced capacity for information storage. This creates an avenue for studying the imprints of the memory burden effect in inflationary cosmology, with the first steps taken in [22].

However, it must be stressed that the situation in de Sitter is very different from the black hole case since there exists no sensible notion of a "stabilized" de Sitter. Instead, as discussed in [22,24], the memory burden gives a consistency upper bound on the duration of classical de Sitter in terms of $t_{\rm M}$. Originally, the bound on the duration of the de Sitter state was derived in [16,25,26] from the self-entanglement of the de Sitter state caused by the back reaction from Gibbons-Hawking radiation.

In this respect, we must notice that the memory burden effect completes a bigger picture of previously suggested mechanisms leading to a breakdown of the semiclassical description for a macroscopic system after a certain critical time, so-called quantum break time [27].

In particular, it has been suggested [16,28] that a black hole experiences quantum breaking while still being macroscopic. This happens the latest after the loss of about half of the initial mass. It has also been argued that at this point, the black hole acquires a significant quantum hair, which could potentially lead to its stabilization [28].

The concept of quantum break time has also been applied to de Sitter [16,25,26]. However, unlike a black hole, which can happily continue the existence beyond this point, the quantum break time represents a consistency upper bound on the duration of any classical de Sitter state. In particular, in any consistent inflationary theory, the inflation must end before the corresponding quantum break time elapses.[1]

The memory burden effect strengthens these earlier quantum break-time proposals for black holes and for de Sitter, as it provides an additional engine for quantum breaking [24]. It also makes the microscopic dynamics of quantum breaking very explicit.

In general, due to its universal nature, the memory burden phenomenon strongly affects the systems with high capacity of information storage, leading to a number of physical consequences.

The rest of this paper is organized as follows. Next section describes the memory burden effect in general systems of enhanced memory storage capacity, which is then specialized to the case of solitons and black holes in Secs. III and IV, respectively. Section V focuses on the analogies and differences between memory burden and classical extremality, while Sec. VI is dedicated to numerical results showing examples of dynamical stabilization of solitons by their memory. Finally, Sec. VII contains remarks on the phenomenological consequences of our findings as well as our outlook. Visuals of our numerical simulations can be found at the following [30,31].

II. ESSENCE OF MEMORY BURDEN

The memory burden effect was introduced in [1], where it was proposed that the loaded information pattern tends to stabilize the system carrying this information. A more detailed analysis of prototype systems was performed in two follow-up papers, [22] and [3], with the purpose of applying the memory burden effect to cosmology and black holes, respectively. The last work concluded that the slowdown of the black hole decay due to the effect is imminent, at the latest, by its half-decay.

In this chapter, following [1,3,22], we shall explain the essence of the memory burden phenomenon and give some helpful classification of its regimes. In order to achieve this, we first go through the main universal characteristics of the systems with the enhanced capacity of information storage. This concept refers to the energetic efficiency of quantum information storage and was introduced in [32–34] at the level of basic Hamiltonians. The reader can find the summary of the setup in [24,35,36].

The main characteristics of effective Hamiltonians describing systems of enhanced information capacity can be determined by categorizing quantum degrees of freedom according to the tasks they perform. The degrees of freedom shall be introduced as quantum oscillators in number representations. These shall later be identified with different modes of the quantum fields.

A. Memory modes

The first category of the degrees of freedom is the memory modes. We shall introduce them as quantum fields denoted by θ^j where the index $j = 1, 2, \ldots, M$ labels their "flavor." The total number of species is M. The corresponding creation-annihilation operators $\hat{a}_j^\dagger, \hat{a}_j$ can satisfy either fermionic or bosonic oscillator algebras.

[1]The quantum inconsistency of an eternally inflating Universe also follows from its incompatibility with the S-matrix formulation of quantum gravity [29].

For definiteness, we shall focus on the bosonic one:

$$[\hat{a}_i, \hat{a}_j^\dagger] = \delta_{ij}, \qquad [\hat{a}_i, \hat{a}_j] = 0. \tag{5}$$

The role of the memory modes is to store information. The information is stored in the patterns of their occupation numbers. These patterns are represented via ket vectors in the Fock space,

$$|p\rangle = |n_1, n_2, \ldots, n_M\rangle, \tag{6}$$

where numbers $n_j \equiv \langle p|\hat{n}_j|p\rangle$ represents the eigenvalues of the corresponding number operators, $\hat{n}_j \equiv \hat{a}_j^\dagger \hat{a}_j$.

The Hilbert subspace formed by the vectors $|p\rangle$ shall be referred to as the memory space. The dimensionality of it is defined by the range of the occupation numbers of the memory modes n_j. These can be subject to constraints.

An example of a simple constraint is to limit each occupation number to two possible values, $n_j = 0, 1$. In this case, the free part of the memory system is described by the Hamiltonian of M independent qubits,

$$\hat{H}_{\text{free}} = \sum_{j=1}^{M} m_j \hat{n}_j, \tag{7}$$

where m_j are the energy gaps of the memory modes. The corresponding dimensionality of the memory space is $n_{\text{st}} = 2^M$. In general, the dimensionality of memory space grows exponentially with the number of memory species M. Thus, the existence of a large number of memory species is an essential condition for the efficiency of information storage. However, it is not sufficient.

Even with large M, the Hamiltonian (7) does not necessarily represent a system of enhanced information capacity. This is because the energy span of the memory space can be very large if the gaps m_j are high.

Therefore, the second important characteristic is the energy cost of an information pattern,

$$E_p = \sum_{j=1}^{M} m_j n_j, \tag{8}$$

as well as the gaps between different memory patterns, $|p\rangle$ and $|p'\rangle$,

$$E_p - E_{p'}. \tag{9}$$

In short, the efficiency of the information storage by a system is determined by the density of states: the number n_{st}, of states $|p\rangle$, that can fit within a physically meaningful smallest energy gap ΔE. Usually, this is set by a typical uncertainty in the system's energy, such as the level width. Naturally, many flavors M and smaller gaps m_j achieve more efficiency.

The resulting information storage capacity is quantified by the microstate entropy of the system defined as

$$S \equiv \ln(n_{\text{st}}). \tag{10}$$

In QFT, the limit to memory capacity is set by saturons [4]: the objects with microstate entropy that saturates the upper bounds (3) and (4) imposed by the validity of a given QFT description.

B. Master modes: Assisted gaplessness

The second category of the degrees of freedom are so-called master modes. We shall denote them by ϕ_α, with creation-annihilation operators, $\hat{a}_{\phi_\alpha}, \hat{a}^\dagger_{\phi_\alpha}$, where $\alpha = 1, 2, \ldots$, is their flavor index.

The role of the master modes is to assist the memory modes in becoming gapless. As opposed to the memory modes, which must come in a large number of flavors M, the number of master mode species can be much less.

To illustrate the mechanism of the assisted gaplessness, and the resulting effect of memory burden, a single flavor of the master mode is sufficient. The corresponding number operator shall be denoted by $\hat{n}_\phi \equiv \hat{a}_\phi^\dagger \hat{a}_\phi$.

With the above conventions, the effect of assisted gaplessness [32–35] can be illustrated by using the following simple prototype Hamiltonian [1,3,22,24],

$$\begin{aligned} \hat{H} &= \hat{H}_{\text{ms}} + \hat{H}_{\text{mem}}, \\ \text{with:}\ \hat{H}_{\text{ms}} &\equiv m_\phi \hat{n}_\phi, \\ \hat{H}_{\text{mem}} &\equiv \left(1 - \frac{\hat{n}_\phi}{N_\phi}\right)^q \sum_j m_j \hat{n}_j, \end{aligned} \tag{11}$$

where, for physical clarity, we have split the Hamiltonian into the master $\hat{H}_{\text{ms}}$ and memory $\hat{H}_{\text{mem}}$ parts, respectively.

The parameters m_ϕ and m_j represent the intrinsic energy (or mass) gaps of the master and memory modes, i.e., the gaps around the Fock vacuum state $n_\phi = n_j = 0$. The number $N_\phi \gg 1$ is a large number that sets the coupling between master and memory modes as $1/N_\phi$. Notice that, in QFT systems, for a given N_ϕ, M is bounded as

$$M \leqslant N_\phi. \tag{12}$$

This bound can be understood as a manifestation of a general bound

$$(\text{coupling}) \times (\text{number of species}) \leqslant 1, \tag{13}$$

violation of which invalidates the QFT description [4]. Thus, within the validity of QFT, the maximal number of memory patterns is achieved for $M \simeq N_\phi$.

The parameter q, which we take as some positive even number, requires clarification. This quantity parametrizes the functional dependence of the effective energy gaps of the memory modes on n_ϕ. Of course, in general, this function can be more complicated. However, near the point of the assisted gaplessness, it is well described by a monomial with a power q. In this form, the assisted gaplessness takes place for the critical occupation number of the master mode,

$$n_\phi = N_\phi. \tag{14}$$

Indeed, if we keep the master mode in the Fock vacuum state, $n_\phi = 0$, and form a memory pattern via the excitations of the memory modes, $|p\rangle = |n_1, \ldots, n_M\rangle$, the cost of energy is

$$E_p = \langle p|\hat{H}_{\rm mem}|p\rangle = \sum_j m_j n_j. \tag{15}$$

This can be extremely high if m_js are large.

However, the system possesses another state (14), with the exact same memory pattern as $|p\rangle$, but with a critically excited memory mode. We shall denote it by $|\tilde{p}\rangle$, where tilde indicates the difference in n_ϕ.

On this state, the contribution to the energy from the memory mode-dependent part of the Hamiltonian is zero:

$$E_{\rm mem} = \langle \tilde{p}|\hat{H}_{\rm mem}|\tilde{p}\rangle = 0. \tag{16}$$

This is because the effective gaps for the memory modes are no longer given by m_j, but rather by the quantities,

$$\omega_j \equiv \left(1 - \frac{n_\phi}{N_\phi}\right)^q m_j, \tag{17}$$

which vanish on a state with $n_\phi = N_\phi$.

Thus, for the information pattern it is energetically favorable that the master mode, instead of being in the vacuum $n_\phi = 0$, is in the critical state $n_\phi = N_\phi$. This is the essence of the mechanism of the assisted gaplessness [32–35] (the term was coined in [35]).

However, the price to pay is the energy of the master mode:

$$E_{\rm ms} = \langle \tilde{p}|\hat{H}_{\rm ms}|\tilde{p}\rangle = m_\phi N_\phi. \tag{18}$$

Due to this, for a given information pattern p, the energetically optimal state is determined by the balance between the two entries $E_{\rm mem}$ and $E_{\rm ms}$. This fixes the occupation number of the master mode, n_ϕ, to a certain optimal value. The energy difference between this optimal state and master mode's Fock vacuum ($n_\phi = 0$), both evaluated for the same memory pattern p, determines the energy efficiency of the information storage.

It is useful to quantify this efficiency by defining the memory-efficiency coefficient as the ratio of the actual cost of an information pattern $E_{\rm mem}$ to its cost in the master mode Fock vacuum:

$$\epsilon \equiv \frac{E_{\rm mem}}{E_p}. \tag{19}$$

Moving away from the above optimal state requires climbing an energetic barrier. This creates a resistance against abandoning the state of the enhanced memory capacity. This is the essence of the memory burden effect [1,3].

C. Memory burden effect

We now wish to give certain universal characteristics of the memory burden effect [1,3,22].

1. Generalities

In order to understand the energetic balance leading to the memory burden effect, let us minimize the Hamiltonian (37) with respect to n_ϕ in a state with a memory pattern $|p\rangle = |n_1, \ldots, n_M\rangle$. The intrinsic (vacuum) energy cost of the pattern, E_p, is given by (15).

Notice that for minimization we can use Bogoliubov approximation in which we treat the operator $\hat{n}_\phi$ as a c number n_ϕ. This is justified, since the occupation number around the states of interest is macroscopic and the c-number approximation of the operator works up to corrections of $1/n_\phi$ (for more detailed discussion of c-number method see [35]).

We can distinguish the two regimes depending on whether E_p is above or below the following critical value,

$$E_* \equiv \frac{1}{q} m_\phi N_\phi. \tag{20}$$

For

$$E_p \geqslant E_*, \tag{21}$$

the minimum of the energy of the system is achieved for

$$n_\phi = N_\phi \left(1 - \left(\frac{E_*}{E_p}\right)^{\frac{1}{q-1}}\right), \tag{22}$$

and it is equal to

$$E = m_\phi N_\phi \left(1 - \frac{q-1}{q}\left(\frac{E_*}{E_p}\right)^{\frac{1}{q-1}}\right). \tag{23}$$

Taking into account (20) and (21), we can easily see that this energy is less than the wouldbe vacuum energy cost of the pattern E_p. That is, in this case, it is energetically

favorable to stabilize the system in the state with nonzero occupation number of the master mode n_ϕ.

On the other hand, for

$$E_p \leqslant E_*, \tag{24}$$

the minimum energy state is

$$n_\phi = 0, \tag{25}$$

with the energy

$$E = E_p. \tag{26}$$

Of course, at the critical value $E = E_*$, the two regimes give the same minimal energy

$$E = E_p = \frac{1}{q} m_\phi N_\phi. \tag{27}$$

That is, if the vacuum energy cost of the pattern is below the critical value (20), it is not worth energetically to keep the system in $n_\phi > 0$ state. Otherwise, the system is stabilized in a state with $n_\phi > 0$ by the memory pattern. This is the key ingredient of the memory burden effect.

Notice, the Hamiltonian (11) conserves the number of the master mode. Correspondingly, the states with arbitrary n_ϕ represent its eigenstates and do not evolve in time. Therefore, in order to observe the stabilizing effect of the memory burden dynamically, we must add interactions that do not conserve n_ϕ and allow for quantum transitions of ϕ quanta into some "external" degrees of freedom $\hat{b}^\dagger, \hat{b}$, with energy gaps m_b. This can be achieved by the inclusion of the interaction terms of the form

$$(\hat{b}^\dagger)^\beta (\hat{a}_\phi)^\alpha + \text{H.c.}, \tag{28}$$

where α, β are integers.

The dynamical memory burden effect is clearly illustrated already in the simplest case $\alpha = \beta = 1$, with $m_\phi = m_b$, which can be solved analytically [1]. The Hamiltonian (11) is supplemented by

$$\hat{H}_{\text{int}} = \frac{\tilde{m}}{\sqrt{N_\phi}} \hat{b}^\dagger \hat{a}_\phi + \frac{\tilde{m}^*}{\sqrt{N_\phi}} \hat{a}_\phi^\dagger \hat{b} + m_\phi \hat{n}_b, \tag{29}$$

where $\hat{n}_b \equiv \hat{b}^\dagger \hat{b}$ is the b-mode number operator and $\tilde{m}$ is a complex parameter of the dimensionality of energy. Notice that $1/\sqrt{N_\phi}$ in the mixing terms makes the parametrization consistent with the normalization of the coupling of the master mode in (11).

The above system can be solved in two ways. We can first find the minimum of energy for a fixed total occupation number

$$n_\phi + n_b = N_\phi, \tag{30}$$

using the Bogoliubov approximation for a_ϕ and b modes. Given the constraint (30), without any loss of generality, we can parameterize these modes replacing the operators by the c-number functions,

$$\hat{a}_\phi = \cos(\theta) e^{i\alpha_\phi} \sqrt{N_\phi}, \qquad \hat{b} = \sin(\theta) e^{i\alpha_b} \sqrt{N_\phi}, \tag{31}$$

where α_ϕ and α_b are phases and θ is an angle that parametrizes the distribution of the occupation number among a_ϕ and b modes. Notice that the phases α_ϕ and α_b drop out of the minimization procedure, since they align with the phase of $\tilde{m}$ and give the negative overall sign of the mixing term.

The total effective Hamiltonian becomes a function of a single variable θ,

$$\hat{H} = \sin(\theta)^{2q} E_p - |\tilde{m}| \sin(2\theta). \tag{32}$$

It is clear that the larger is E_p, the closer is the minimum of the energy to $\theta = 0$, which implies $n_\phi = N_\phi$ and $n_b = 0$.

For $qE_p/|\tilde{m}| \gg 1$, the system gets stabilized in the state of enhanced memory capacity with the depleted number of master modes, $\Delta n_\phi = N_\phi - n_\phi$, given by

$$\frac{\Delta n_\phi}{N_\phi} = \sin^2\theta \simeq \left(\frac{|\tilde{m}|}{qE_p}\right)^{\frac{2}{2q-1}}. \tag{33}$$

Correspondingly, this number gets transferred to the b mode.

On the other hand, for $E_p = 0$, the minimum is achieved for $\theta = \pi/4$ implying that the average occupation numbers satisfy

$$n_\phi = n_b. \tag{34}$$

These results are fully confirmed by the explicit quantum evolution of the system.

Indeed, following [1,3], let us time evolve the system from the initial state $n_\phi = N_\phi$ and $n_b = 0$.

For $E_p = 0$, the occupation numbers evolve in time as

$$\frac{n_\phi(t)}{N_\phi} = \cos^2\left(\frac{|\tilde{m}|}{\sqrt{N_\phi}} t\right), \qquad \frac{n_b(t)}{N_\phi} = \sin^2\left(\frac{|\tilde{m}|}{\sqrt{N_\phi}} t\right), \tag{35}$$

which, for the averaged values, reproduce (34).

For $qE_p/|\tilde{m}| \gg 1$, the story is very different. The oscillation amplitude is now suppressed, so that the average value of Δn_ϕ is given exactly by (33). For a detailed numerical analysis, see [3].

Of course, the above example of the system's decay represents an oversimplified toy model, with the main purpose of illustrating the system with a swift memory

burden effect. The time evolution must be taken with a grain of salt, especially in the later oscillatory period.

For QFT systems, such as a black hole or a soliton, submerged in infinite space, the master mode can decay into a continuum of the external b modes. These correspond to different momentum (or spin) eigenstates of outgoing radiation. In such cases, the time evolution of the system is dissipative rather than oscillatory. Regardless, as long as the system maintains the information pattern with $E_p \gg m_\phi$, it is subjected to memory burden, latest for $\Delta n_\phi / N_\phi \sim 1$. That is, the memory burden phase starts latest by the time the system gets rid of an order-one fraction of its initial energy.

The way of avoiding the memory burden would be for the system to get rid of the information pattern very fast [1]. However, in systems of enhanced information capacity, due to the assisted gaplessness, this is an extremely suppressed process [3]. For a detailed numerical analysis of complex prototype systems, demonstrating this outcome, the reader is referred to the above paper.

We now move to discussions of different parameter regimes and distinguish the two extreme realizations of the memory burden effect.

2. Type-I regime

The first regime, which we call type I, takes place when the intrinsic frequencies of the master and memory modes are of the same order. We shall take them to be given by an universal mass gap m:

$$m = m_\phi = m_j. \tag{36}$$

The Hamiltonian (11) becomes

$$\hat{H} = m\hat{n}_\phi + m\left(1 - \frac{\hat{n}_\phi}{N_\phi}\right)^q \sum_{j=1}^{M} \hat{n}_j. \tag{37}$$

Notice that it is invariant under an arbitrary $U(M)$ transformation of the memory modes: $\hat{a}_j \to U_{jk}\hat{a}_k$.

Let us evaluate the Hamiltonian on a memory pattern, with total occupation number of all species given by

$$\sum_{j=1}^{M} n_j = N_{\rm G}. \tag{38}$$

Due to $U(M)$ symmetry this number can be arbitrarily redistributed among M memory modes, which creates the following number of degenerate microstates [4],

$$n_{\rm states} \simeq \left(1 + \frac{N_{\rm G}}{M}\right)^M \left(1 + \frac{M}{N_{\rm G}}\right)^{N_{\rm G}}. \tag{39}$$

The above expression represents a binomial coefficient $\binom{N_{\rm G}}{M}$ evaluated using Stirling approximation for large $N_{\rm G}$ and M.

This degeneracy can be understood in terms of the Goldstone phenomenon, since the occupation number of modes $N_{\rm G}$ breaks the $U(M)$ symmetry spontaneously down to $U(M-1)$.

The memory pattern back reacts on the master mode. In order to understand this backreaction, following [34], we minimize the Hamiltonian (37) with respect to n_ϕ. This gives

$$\left(1 - \frac{n_\phi}{N_\phi}\right)^{q-1} = \frac{N_\phi}{qN_{\rm G}}. \tag{40}$$

We see that for $N_{\rm G} \geqslant N_\phi$, $n_\phi \simeq N_\phi$. Plugging (40) in the generic expression (17) for the effective gaps of the memory modes, we get

$$\omega = m\left(\frac{N_\phi}{qN_{\rm G}}\right)^{\frac{q}{q-1}}. \tag{41}$$

In particular, for $q \gg 1$, we obtain

$$\frac{\omega}{m} \simeq \frac{N_\phi}{qN_{\rm G}}. \tag{42}$$

Notice also that the contribution to the energy from the master and memory modes

$$E_{\rm ms} = mN_\phi, \qquad E_{\rm mem} = \omega N_{\rm G} \tag{43}$$

relate as

$$E_{\rm mem} \simeq \frac{1}{q} E_{\rm ms}. \tag{44}$$

From (43) and (42), it is clear that, in type I, the memory-efficiency coefficient is

$$\epsilon_I \simeq \frac{\omega}{m} \simeq \frac{N_\phi}{qN_{\rm G}}. \tag{45}$$

In realistic systems, due to interactions with external degrees of freedom, the occupation number n_ϕ can change in time. In the previous section we reproduced an example of [34] in which the transition takes place into a single b mode. In this case, the behavior is oscillatory. However, when the number of external decay channels is large, the inverse transitions practically never happen and n_ϕ decreases irreversibly.

For example, this is what happens in black holes [3], where the master mode gets depleted into outgoing Hawking particles [14]. In such cases, the system dynamically evolves until it gets stabilized (or semistabilized) by the memory burden effect.

In other words, the information drives the system towards the state in which the energy cost of the information pattern is optimal. Correspondingly, the system resists against the attempts of driving it away from such a state. We shall later discuss this dynamics in solitons and in black holes and compare them.

3. Type-II regime

We shall now consider the regime in which the intrinsic energy gaps of the memory modes are much higher than that of the master mode:

$$m_j \gg m_\phi. \tag{46}$$

We shall refer to it as type II. In this case the minimization of the Hamiltonian with respect to n_ϕ gives

$$\left(1-\frac{n_\phi}{N_\phi}\right)^{q-1} = m_\phi \frac{N_\phi}{qE_p}. \tag{47}$$

Taking into account (13) and (46), we notice that for a memory pattern with $N_{\rm G} \gtrsim M$, the rhs, of the above equation is much less than one. Thus, similarly to type-I case, we have $n_\phi \simeq N_\phi$. Correspondingly, the energy cost of the master mode is

$$E_{\rm ms} \simeq m_\phi N_\phi. \tag{48}$$

At the same time, the actual energy cost of the memory pattern is

$$E_{\rm mem} = \left(m_\phi \frac{N_\phi}{qE_p}\right)^{\frac{q}{q-1}} E_p \simeq \frac{1}{q} m_\phi N_\phi. \tag{49}$$

Thus, we arrive to the same relation (44) as in type-I case.

However, the efficiency coefficient ϵ is now extra suppressed. For example, taking all m_j to be set by a single scale, $m_j = m \gg m_\phi$, we get

$$\epsilon_{II} \equiv \frac{N_\phi}{qN_{\rm G}} \frac{m_\phi}{m}. \tag{50}$$

This is suppressed with respect to type-I case (45) by an additional factor m_ϕ/m.

The basic lesson is the following: Increasing the vacuum gaps of the memory modes with respect to the master mode, the system becomes more and more efficient in information cost. Correspondingly, the memory burden effect is stronger.

III. MEMORY BURDEN IN SOLITONIC SATURON

We shall now study the memory burden effect in solitonic saturons. Following [4], we first introduce an example of a saturon in form of a vacuum bubble. Next, we discuss their stabilization via memory burden effect closely following [10].

The bubble is a solution in a renormalizable $SU(N)$-invariant theory of a scalar field Φ in the adjoint representation with the following Lagrangian density,

$$\mathcal{L}[\Phi] = \frac{1}{2}{\rm Tr}(\partial_\mu \Phi)(\partial^\mu \Phi) - V(\Phi), \tag{51}$$

where the potential is chosen as

$$V(\Phi) = \frac{\alpha}{2}{\rm Tr}\left(f\Phi - \Phi^2 + \frac{I}{N}{\rm Tr}\Phi^2\right)^2. \tag{52}$$

Here α is a coupling constant and f is a scale. I is an unit matrix in $SU(N)$ space.

The validity of QFT description imposes the following bound on the parameters of the model,

$$\alpha N \lesssim 1. \tag{53}$$

Basically, the quantity αN, which is analogous to 't Hooft coupling, must not exceed the critical value. In the opposite case ($\alpha N \gg 1$), Φ no longer represents a good QFT degree of freedom. This is unambiguously signaled by the breakdown of the loop expansion, as well as, by the saturation of unitarity in multiparticle scattering amplitudes [4]. Notice that after we map the above theory on a generic Hamiltonian of enhanced memory capacity (11), it will become clear that the bound (53) represents a particular case of the bound (13).

The system (51) has multiple degenerate vacua satisfying the condition

$$f\Phi^b_a - (\Phi^2)^b_a + \frac{\delta^b_a}{N}{\rm Tr}\Phi^2 = 0. \tag{54}$$

We shall focus on a pair of neighboring vacua.

In the first one, the vacuum expectation value is $\Phi = 0$ and the global $SU(N)$ symmetry is unbroken. This vacuum exhibits a mass gap

$$m = \sqrt{\alpha} f, \tag{55}$$

which sets the minimal energy cost for all particle excitations.

In the second vacuum of our interest, the vacuum expectation value is

$$\Phi_0 = f\frac{1}{\sqrt{N(N-1)}}{\rm diag}(N-1,-1,\ldots,-1), \tag{56}$$

and $SU(N)$ symmetry is spontaneously broken down to $SU(N-1)\times U(1)$. Due to spontaneous breaking of symmetry, in this vacuum we have the set of massless Goldstone bosons

$$\theta^j(x), \quad j = 1, 2, \ldots, M, \tag{57}$$

corresponding to broken generators T^j. Their total number is

$$M = 2(N-1). \tag{58}$$

These Goldstones form a fundamental representation of the $SU(N-1)$ group of complex dimensionality $N-1$ with nonzero charge under $U(1)$.

The effective Lagrangian of the Goldstone bosons has the following form:

$$\mathcal{L}_{\text{eff}} = f^2(\partial_\mu \mathcal{U}(x))(\partial^\mu \mathcal{U}(x)), \tag{59}$$

with

$$\mathcal{U}(x) \equiv f^{-1} U(x)^\dagger \Phi_0 U(x), \tag{60}$$

where $U(x)$ is the space-time dependent $SU(N)$-transformation matrix,

$$U(x) = \exp\left[-i\theta^j(x) T^j\right]. \tag{61}$$

Up to second order in $\theta^j(x)$ s and leading order in $1/N$, the Goldstone Lagrangian can be written as

$$\mathcal{L}_{\text{eff}} \simeq \frac{1}{4} f^2 \sum_j (\partial_\mu \theta^j)(\partial^\mu \theta^j). \tag{62}$$

A. Vacuum bubbles

Due to the degeneracy of vacua, there also exist the domain wall configurations separating them,

$$\Phi(x) = \phi(x) \frac{1}{\sqrt{N(N-1)}} \text{diag}(N-1, -1, \ldots, -1), \tag{63}$$

where the function $\phi(x)$ interpolates between 0 and f. We shall be interested in a spherically symmetric bubble (closed wall) of $\phi = f$ vacuum embedded in $\phi = 0$ one.

Let us first consider the following configuration,

$$\Phi = \frac{\phi(r,t)}{f} \Phi_0. \tag{64}$$

The field $\phi(r,t)$ satisfies the following equation of motion:

$$\partial_t^2 \phi - \partial_r^2 \phi - \frac{2}{r} \partial_r \phi + \frac{\partial V}{\partial \phi} = 0, \tag{65}$$

where

$$V(\phi) = \frac{\alpha}{2} \phi^2 (\phi - f)^2. \tag{66}$$

The boundary conditions are such that for $t = 0$, $\phi(r = \infty) = 0$ and $\partial_t \phi|_{t=0} = \partial_r \phi|_{r=0} = 0$.

If the initial radius of the bubble satisfies $R \gg m^{-1}$, then red the initial configuration can be approximated by

$$\phi(r) = \frac{f}{2}\left[1 + \tanh\left(\frac{m(R-r)}{2}\right)\right]. \tag{67}$$

The bubble wall has a thickness $\delta_w \simeq m^{-1}$ and a tension, $\sigma \simeq m^3/(6\alpha)$. Order of magnitude wise, this remains true also for thick-walls bubbles for which $R \sim \delta_w$.

In the interior of the bubble, the $SU(N)$ symmetry is broken spontaneously down to $SU(N-1) \times U(1)$. Due to this, there are $M = 2(N-1)$ gapless Goldstone species localized within the bubble. These species do not exist outside of the bubble, since $SU(N)$ symmetry is restored there.

As a consequence, the bubble has a large microstate degeneracy. This degeneracy follows from spontaneously broken $SU(N)$ symmetry, since a bubble obtained from (63) by an arbitrary red and general $SU(N)$ transformation U,

$$\Phi(x) \to U^\dagger \Phi(x) U, \tag{68}$$

represents a classical solution of the same energy.

In quantum theory, the number of degenerate microstates is not infinite, since only the orthogonal states must be counted. These states are obtained by redistribution of the constituent quanta of the bubble among different $SU(N)$ flavors, which (in large-N) amounts to the following number of degenerate microstates [4],

$$n_{\text{states}} \simeq \left(1 + \frac{s(R)}{2N}\right)^{2N} \left(1 + \frac{2N}{s(R)}\right)^{s(R)}, \tag{69}$$

where the quantity $s(R) = 4\pi(Rm)^3/\alpha$ is the time-averaged space integral of red $\phi^2(r,t)$ over an oscillation/pulsation period. This quantity effectively measures the mean occupation number of constituent quanta of the bubble soliton viewed as a coherent state [37].

Taking the maximal value of N given by (53), for thick-wall bubbles $R \sim 1/m$, we get the following expression for entropy,

$$S \sim N \sim \frac{1}{\alpha}. \tag{70}$$

It is clear that this expression represents the area ($\sim 1/m^2$) in units of the Goldstone scale f. Thus, for thick wall bubbles the entropy saturates the area-law bound (4).

For $R \gg 1/m$, the entropy is

$$S \sim N \ln(mR). \tag{71}$$

Due to the above degeneracy, the bubble represents a system of enhanced capacity of the memory storage. The memory modes are Goldstone modes θ^j. The master mode is the radial mode, $\phi(x)$.

Setting other components to zero, the effective Lagrangian of Goldstone modes and of the radial mode ϕ is given by

$$\mathcal{L}_{\text{eff}} = \frac{1}{2}\partial_\mu\phi\partial^\mu\phi + \frac{1}{2}\phi^2(\partial_\mu\mathcal{U}(x))(\partial^\mu\mathcal{U}(x)) - V(\phi). \tag{72}$$

The Goldstone modes are well defined, unless $\phi \neq 0$.

B. Stabilization by memory burden

We can now observe the stabilization by the memory burden effect. In this, we shall closely follow [10], where this effect was studied. This effect requires that a nonzero information pattern is stored in nonzero frequency excitations of Goldstone modes. That is, some of the Goldstone modes (i.e., the memory modes) of nonzero frequencies are occupied to numbers n_a.

On such a state, $|p\rangle \equiv |n_1, n_2, \ldots, n_M\rangle$, the measure of the memory burden effect is the expectation value,

$$\langle p|(\partial_\mu\mathcal{U}(x))(\partial^\mu\mathcal{U}(x))|p\rangle. \tag{73}$$

In order to understand the effect, let us first consider a classical configuration (60) with

$$U = e^{it\omega_j T^j}. \tag{74}$$

It is easy to see that this gives the equation

$$\partial_t^2\phi - \partial_r^2\phi - \frac{2}{r}\partial_r\phi - \omega^2\phi + \frac{\partial V}{\partial\phi} = 0, \tag{75}$$

with

$$\omega^2 \equiv \sum_{j=1}^{M}\omega_j^2. \tag{76}$$

Different patterns $(\omega_1, \omega_2, \ldots)$ can be obtained from one another by $SU(N-1)$ transformation, which leaves the Φ_0 invariant.

The above equation always has a stationary bubble solution with time-independent $\phi(r)$. The asymptotic values are $\phi(\infty) = 0$ and $\phi(0) \neq 0$. Since various patterns $(\omega_1, \omega_2, \ldots, \omega_M)$ are related by a symmetry transformation, it is sufficient to discuss the case $\omega^j = \delta^{j1}\omega$ and later generalize to different patterns.

In the thin-wall limit, $R \gg 1/m$, the profile of the bubble is given by (67), where the radius R can be determined by extremizing the energy of the bubble as function of R,

$$E = \frac{2\pi}{3\alpha}m^3R^2(1-\dot{R}^2)^{-1/2} + \frac{2\pi}{3\alpha}m^2\omega^2R^3, \tag{77}$$

subject to the condition that the quantity

$$Q = \frac{2\pi}{3}f^2\omega R^3 = \frac{2\pi}{3\alpha}m^2\omega R^3 \tag{78}$$

represents a conserved charge. This determines the radius of the stationary bubble as

$$R_0 = \frac{2}{3}\frac{m}{\omega^2}. \tag{79}$$

Correspondingly, the energy of the bubble is

$$E_0 = \frac{\omega}{\alpha}\frac{m^5}{\omega^5}\left(\frac{40\pi}{81}\right). \tag{80}$$

As already discussed in [10], the stationary bubble solution can be mapped on a $U(1)$ nontopological soliton or a Q ball [38–40] formed by a complex scalar with modulus $\phi(r)$ and the $U(1)$-charge Q given by (78) (for some implications of Q balls, see, e.g., [41–48]). However, despite the similarity of classical solutions, such a soliton will not exhibit a significant microstate degeneracy and will not represent a system of enhanced capacity of information storage. Correspondingly, the charge Q cannot be associated with any information pattern. For a significant microstate degeneracy, having $SU(N)$ symmetry is crucial. Only in such a case the total charge Q can be distributed among an exponentially large number of memory patterns.

The stationary bubbles carrying arbitrary patterns are obtained by $SU(N-1)$ transformations and have identical macroscopic features such as the energy and the radius. However, they have different characteristics with respect to an asymptotic probe with fixed $SU(N-1)$ quantum numbers relative to which the rotation is performed.

In other words, the information is stored in $SU(N-1)$ rotations of a pattern relative to a fixed observer. Obviously, all rotated bubbles have identical energies, but they are distinguished by the observer who can perform a scattering experiment using a fixed probe.

The stationary bubble represents a bubble stabilized by the memory burden effect. In terms of occupation numbers of Goldstones, n_j, the quantities ω_j read

$$\omega_j^2 = \omega n_j \frac{3}{2\pi f^2 R_0^3}. \tag{81}$$

From the quantum perspective, it is illuminating to express the energy of the bubble in terms of the occupation

numbers of the radial (master) mode, N_ϕ, and of the Goldstone modes

$$N_{\rm G} \equiv \sum_{j=1}^{M} n_j. \tag{82}$$

Splitting the energy of the stationary bubble (80) into two contributions, we have

$$E_0 = E_{\rm mem} + E_{\rm ms}, \tag{83}$$

where

$$E_{\rm mem} = \omega N_{\rm G}, \quad \text{with,} \quad N_{\rm G} \equiv \frac{1}{\alpha}\frac{m^5}{\omega^5}\left(\frac{16\pi}{81}\right), \tag{84}$$

is the energy of memory (Goldstone) modes, whereas

$$E_{\rm ms} = mN_\phi, \quad \text{with} \quad N_\phi \equiv \frac{1}{\alpha}\frac{m^4}{\omega^4}\left(\frac{8\pi}{27}\right) \tag{85}$$

is the energy of the master (radial) mode $\phi(r)$. At the stationary point we have

$$E_{\rm mem} = \frac{2}{3}E_{\rm ms}. \tag{86}$$

Notice that this reproduces the generic equation (44) with $q = 3/2$.

From (78) and (84) it is easy to notice that we have

$$Q = N_{\rm G}. \tag{87}$$

That is, the classical charge in quantum theory counts the total occupation number of Goldstone modes. Various memory patterns are obtained by distribution of $N_{\rm G}$ among $M = 2(N-1)$ flavors of Goldstones.

Next, notice that the memory pattern with the same $N_{\rm G}$ in the $SU(N)$-invariant vacuum would cost

$$E_p = mN_{\rm G}, \tag{88}$$

since in this vacuum the minimal energy gap of any elementary excitation with $SU(N)$ quantum number is m.

Taking this into account, we can evaluate the memory-efficiency coefficient (19), which gives

$$\epsilon = \frac{\omega}{m} \simeq \frac{2N_\phi}{3N_{\rm G}}. \tag{89}$$

In the last equality we have expressed ω/m through occupation numbers via (84) and (85). This reproduces Eq. (45) with $q = 3/2$. We thus see that the vacuum bubble realizes the type-I memory burden effect, with $q = 3/2$.

The type-I nature of the memory burden is not surprising, since in the $SU(N)$ invariant vacuum, the energy gaps of all excitations are equal to m.

The stationary bubble represents a bubble stabilized by the memory burden. Notice that for such a bubble we have

$$Q = N_{\rm G} = \frac{\pi}{\alpha}(mR_0)^{5/2}\left(\frac{2}{3}\right)^{3/2}. \tag{90}$$

A bubble with an insufficient memory burden will not be stationary. In particular, such is a bubble with the radius larger than the critical value $R \gg R_0$. Obviously, for such a bubble,

$$N_{\rm G} \ll \frac{\pi}{\alpha}(mR_0)^{5/2}\left(\frac{2}{3}\right)^{3/2} \tag{91}$$

and

$$E_{\rm mem} \ll \frac{2}{3}E_{\rm ms}. \tag{92}$$

The memory burden is insufficient for stabilizing such a bubble. Instead, as shown in [10], the bubble starts to collapse and oscillate emitting energy. This decreases the occupation number of the master mode. This process shall continue until the balance is restored to (86). At this point the bubble gets stabilized by the memory burden effect.

In particular, the initial bubbles of equal energies but different values of $N_{\rm G}$ will evolve into the stabilized bubbles of different energies as we shall discuss next.

C. The energy splitting by memory burden

We wish to discuss the following important effect which is characteristic of the phenomenon of memory burden stabilization. Namely, the initially degenerate energy states with different memory patterns $N_{\rm G} \neq N'_{\rm G}$, upon stabilization by the memory burden, split in energies.

Let us start with two initial bubble states with different values of the Goldstone occupation numbers, $N_{\rm G}$ and $N'_{\rm G}$, respectively. We assume that both numbers are subcritical (91). Thus, initially the memory burdens are dynamically insignificant. According to (93), the contribution to the energy from the memory modes is

$$E_{\rm mem} = \omega N_{\rm G} \sim N_{\rm G}\sqrt{\frac{m}{R}}. \tag{93}$$

Notice that order-of-magnitude wise this expression holds also for (91), since $\omega \sim \sqrt{\frac{m}{R}}$.

Correspondingly, the energy splitting between the two bubble states with fixed difference, $\Delta N_{\rm G} \equiv N_{\rm G} - N'_{\rm G}$,

$$\Delta E \sim \Delta N_{\rm G}\sqrt{\frac{m}{R}}, \tag{94}$$

vanishes for $R \to \infty$. Thus, for sufficiently large and equal radii, the two bubble states are nearly degenerate.

Notice that the states with different $N_{\rm G}$ are fully legitimate microstates of the same macrostate. Semiclassically, the detection of the Goldstone charge is not possible. In quantum theory any attempted measurement is suppressed by powers of $\Delta N_{\rm G}/N_\phi$, which vanishes in the semiclassical limit. Thus, the microstates with different $N_{\rm G}$ are equally indistinguishable semiclassically as the microstates with equal $N_{\rm G}$ but relatively rotated in $SU(N)$ space.

Now, since the occupation numbers of Goldstones, $N_{\rm G}, N'_{\rm G}$, are subcritical (91), the bubbles will evolve in time by oscillating and emitting energy until they get stabilized by the memory burden effects. Since during this process the radii diminish and correspondingly the Goldstone frequencies (ω) grow, so does the energy splitting between the two bubble states.

At the stabilization point, the bubble energies can be highly split if the relative difference of Goldstone numbers is large. For example, for $\Delta N_{\rm G}/N_{\rm G} \sim 1$, the energy splitting between the two bubble "remnants" is of order their masses. Of course, the energy of a remnant plus radiation is the same in both cases.

To summarize: For a soliton that has not yet entered the memory burden stabilization phase [i.e., an underburdened soliton with (91)], we can distinguish the two types of degenerate microstates: (1) the microstates that have the same memory burden $N_{\rm G}$ and (2) the microstates with different values of $N_{\rm G}$.

The first category belongs to the same orbit in $SU(N)$ space and, therefore, remains degenerate throughout the bubble evolution. However, the energies of the second category undergo the splittings according to (94).

The above situation is generic for the memory burden effect. In particular, as we shall discuss, the same phenomenon takes place in black holes. There too, after entering the memory burden domination phase, the masses of initially degenerate black holes with different information patterns can become vastly different—see Fig. 1 for a schematic visual. We shall also demonstrate this effect numerically in Sec. VI.

Finally, we wish to stress that while the memory burden stabilizes the systems, the converse is not excluded: the stable systems with very little information capacity can happily exist. An example of such a system would be the Q ball with the $U(1)$ charge. Although the $U(1)$ charge carries very little information, it nevertheless can stabilize the system dynamically.

The important thing about the systems with high information content (such as saturons) is that they have no choice: the memory burden effect stabilizes them necessarily.

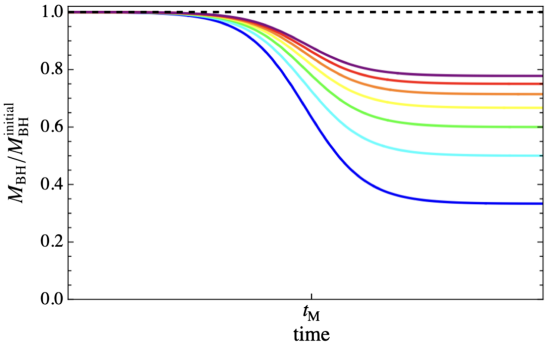

FIG. 1. Schematic view of the splitting of energies of the microstates of either a soliton or a black hole, time evolved from initially (nearly) degenerate microstates with different memory patterns. The solid lines represent the energies of the remnant states, whereas the black dashed line represents the total energy of the system (the remnant mass plus the energy of emitted radiation). Notice that each solid line is not a single state but accounts for all the states that remain degenerate due to identical memory burdens. The degeneracy can be exact due to symmetry. For example, such are the vacuum bubble microstates related by $SU(N)$ symmetry. The line can also exhibit a finer structure, in case the symmetry is only approximate.

IV. MEMORY BURDEN IN BLACK HOLES

Already in the original papers on memory burden [1,3,22] it has been argued that black holes must be subjected to this phenomenon. Furthermore, the analysis of [3] revealed that the stabilizing nature of the effect, with high likelihood, leads to the prolongation of black hole's lifetime. Here, we shall further scrutinize this question in light of our analysis.

Let us first structure the arguments that justify the presence of the memory burden effect in black holes. This conclusion can be reached by three independent lines of evidence.

The first line developed in [1,3] is based on the universality of the phenomenon. The review of the effect given in Sec. II makes it evident that it is impossible to construct a Hermitian Hamiltonian with efficient information storage that avoids the memory burden phenomenon. The fact that the black holes are efficient (in fact, the most efficient) storing devices, indicates that the effect must be present there.

Further justification is provided by the analysis of [10] and by its continuation in the present work. This analysis shows the presence of the memory burden effect in solitonic saturons. These objects share with black holes all the known key features such as information horizon, area-law entropy, thermal decay, and Page-like time of information retrieval. This gives a strong indication that memory burden must belong to this list.

Finally, the third line of reasoning is based on hints from a microscopic theory, a so-called black hole's quantum N portrait [14–16]. According to this theory, a black hole

represents a saturated coherent state (or a condensate) of gravitons, at criticality. The term criticality implies that the mean occupation number is inverse of the gravitational coupling. In the present language, these coherent gravitons play the role of a master mode. This theory offers a microscopic explanation of black hole properties within the domain of calculability.

In particular, the entropy of a black hole is explained by the emergence of M "flavors" of the gapless modes in the above critical state of gravitons. These can be described as Bogoliubov/Goldstone modes of the critical graviton condensate [15,49–51].

In the present language, they represent the memory modes. In our reasoning of establishing the nature of the memory burden in black holes, we shall borrow only very general features of N portrait, as this was done in [1,3]. We shall stay strictly within the calculability domain of the QFT framework.

Namely, we shall rely on the following rather conservative (and natural) starting points:

(1) Both memory and master modes of a black hole are describable as modes of the graviton field. Although additional field species can certainly exist, e.g., in form of string excitations, they do not change the essence of the effect (although, can lead to certain modifications [24]). We come to the role of the extra species later, in Sec. IV C.

(2) The memory modes can be classified according to the symmetries that are left unbroken by the black hole metric. This is analogous to how in our bubble example the Goldstone memory modes have been characterized by their quantum numbers under the $SU(N-1)\times U(1)$ unbroken symmetry.

Equipped with the above guidelines, we shall discuss the black hole memory burden effect. Let us first identify the master and memory modes.

The identification of the master mode is easy, since at the initial times, this mode has macroscopic occupation number and is therefore well-described classically. Moreover, since the Bogoliubov approximation works for such modes, as a control parameter we can use the suitable characteristics of the classical metric. Basically, the master modes are Fourier harmonics of the classical metric. For a black hole of radius R, the dominant contribution comes from the modes of energy gap,

$$m_\phi \sim 1/R. \tag{95}$$

Of course, the black hole metric viewed as the coherent state of gravitons is a distribution peaked around the above value [14]. For our purposes, it suffices to consider a single mode rather than a sharply peaked distribution.

Let us now identify the memory modes. As already said, we shall only use very general points outlined above. We know that the memory modes must come from graviton modes and can be classified according to symmetries of the classical metric. Moreover, the number of their flavors, M, must be

$$M \sim S_{\rm BH}, \tag{96}$$

where $S_{\rm BH}$ is the Bekenstein-Hawking entropy which for a black hole of mass $M_{\rm BH}$ and radius R is [2]

$$S_{\rm BH} = \pi (R M_{\rm P})^2 = 4\pi \frac{M_{\rm BH}^2}{M_{\rm P}^2}. \tag{97}$$

There exist unique candidates fulfilling the above requirements that can emerge as the assisted gapless modes [1,33]. These are the modes of the graviton corresponding to various spherical harmonics, Y_{lm}. Only the harmonics with momenta up to cutoff of the theory must be included, since only such modes are the legitimate (weakly coupled) QFT degrees of freedom. In Einstein gravity, with no additional light species besides graviton, the cutoff is $M_{\rm P}$. We thus need to include all possible spherical harmonics of graviton up to the Planck mass.

For a black hole of radius R, this counting gives the multiplicity of memory flavors that scales as the area of a black hole in units of $M_{\rm P}$,

$$M \sim (R M_{\rm P})^2, \tag{98}$$

and therefore precisely matches the entropy demand (97) [1,33].

As an additional supporting evidence, the above fully matches the counting of gapless modes from the black hole symmetries derived in [51,52].

Of course, the majority of modes comes from the highest spherical harmonics. We thus identify the gapless memory modes of a black hole as the modes of angular momenta $\sim M_{\rm P} R$. Their counterparts in the asymptotic vacuum are the same angular harmonics Y_{lm} of a free graviton. However, these carry the energy gaps $m_j \sim M_{\rm P}$.

Notice that the above explains why a black hole cannot emit information efficiently [1]: in order to "escape" from a black hole via a quantum process, a memory mode has to climb an extremely high energetic barrier.

The existence of modes with the same Y_{lm} but with largely split energy gaps inside and outside of a black hole is not surprising. The black hole breaks the Poincare symmetry at the scale $M_{\rm P}$ [4]. Due to this, the memory modes of a black hole, despite having the high orbital momenta, are gapless, whereas the asymptotic modes with similar momenta are gapped by $\sim M_{\rm P}$.

The above knowledge suffices for adapting the generic Hamiltonian (11) to a black hole situation. The effective Hamiltonian of black hole memory and master modes is described by (11) with the understanding that index j labels spherical harmonics Y_{lm}. Correspondingly, the intrinsic

gaps of master and memory modes are

$$m_\phi \sim \frac{1}{R} \quad \text{and} \quad m_j \sim M_{\rm P}, \tag{99}$$

respectively. The coupling of the master mode to memory modes is set by the standard gravitational coupling $\alpha_{\rm gr}(R)$ evaluated at scale R,

$$\frac{1}{N_\phi} \sim \alpha_{\rm gr}(R) \sim \frac{1}{(RM_{\rm P})^2}. \tag{100}$$

As pointed out in [14], this coupling is equal to the inverse of the Bekenstein-Hawking entropy $S_{\rm BH}$. This is not an accident. As explained in [4], this equality puts $S_{\rm BH}$ in accordance with the generic bound on entropy (3).

Now, in this description, the initial state of a classical black hole corresponds to the critical state $n_\phi = N_\phi$ in which the memory modes are essentially gapless, $\omega_j = 0$.

As already discussed in [1], this explains why at the initial stages of evaporation, the black hole information cannot come out. Indeed, due to the conservation of the angular momentum, translating the information stored in the memory modes into the asymptotic quanta, would require radiating the quanta of energies $\sim M_{\rm P}$, which is not possible. In addition, a pair-wise annihilation of memory modes of frequencies ω into the soft (low angular momentum) external quanta is suppressed as $\sim\omega_j^5/M_{\rm P}^4$ and is negligible (see below). Thus, neither the emission of the memory modes nor their conversion into the external quanta is an option.

At the same time, the black hole can emit the master mode via quantum scattering, reproducing the ordinary Hawking radiation [53]. Basically, the process is a conversion of a master mode into asymptotic quanta of similar frequencies. This process is unsuppressed, since the occupation number of the master mode is equal to its inverse coupling. As a result, the suppression by powers of coupling is compensated by the occupation number, and the rate of emission is [14]

$$\Gamma_{\rm ms} \sim \frac{1}{R}\frac{n_\phi^2}{N_\phi^2} \sim \frac{1}{R}, \tag{101}$$

which reproduces the Hawking rate. This simple quantum explanation of the Hawking effect is one of the successes of N portrait [14]. However, due to generic nature of the effect, it holds for arbitrary saturons [9,10].

Since we start in the critical state $n_\phi = N_\phi$, at the initial stages the memory burden effect is weak. At this stage, Eq. (101) is a good approximation. It tells us that, on average, n_ϕ decreases by $\Delta n_\phi \sim 1$ over time $\Delta t \sim R$.

As is obvious from (11), in general, decreasing the occupation number of the master mode by Δn_ϕ affects its gap by

$$\Delta m_\phi \sim \frac{q}{N_\phi}\left(\frac{\Delta n_\phi}{N_\phi}\right)^{q-1} E_p. \tag{102}$$

Taking into account (99), (100) and $N_{\rm G} \sim M \sim S_{\rm BH}$, this is of the order

$$\Delta m_\phi \sim q\left(\frac{\Delta n_\phi}{N_\phi}\right)^{q-1} M_{\rm P}. \tag{103}$$

The memory burden effect becomes dominant by the time when $\Delta m_\phi \sim 1/R$, which gives

$$\frac{\Delta n_\phi}{N_\phi} = (qM_{\rm P}R)^{-\frac{1}{q-1}}. \tag{104}$$

The same expression is obtained from (47) after taking into account (99).

The effective gaps of the memory modes also grow with Δn_ϕ as

$$\omega_j = \left(\frac{\Delta n_\phi}{N_\phi}\right)^q M_{\rm P}, \tag{105}$$

and by the time of validity of (104), they become

$$\omega_j = \frac{1}{qR}\frac{1}{(qM_{\rm P}R)^{\frac{1}{q-1}}}. \tag{106}$$

In the above expressions, the quantities R and $S_{\rm BH}$ must be understood as the parameters of the initial black hole.

We must remember that we track the evolution of an initial state with a given memory pattern. The microstate entropy $S_{\rm BH}$ accounts for the degeneracy of various patterns. However, as the evolution goes on and memory modes gain energy gaps, the initially degenerate memory patterns get split in energy. Of course, the total energies of the systems, i.e., black hole plus radiation, obtained by evolving different initial patterns, are degenerate. However, the fractions of energy that remain stored in the black hole relative to radiated portion are different for states evolved from different initial patterns (see Fig. 1).

Equations (104) and (106) determine the onset of the memory burden using as a clock the change in occupation number of the master mode Δn_ϕ. Since before the onset of the memory burden effect, this number changes by usual Hawking emission, essentially it measures the time in units of R: $t = \Delta n_\phi R$.

It also measures the onset of memory burden in terms of the emitted fraction of the initial mass of a black hole as $\Delta M_{\rm BH}/M_{\rm BH} = \Delta n_\phi/N_\phi$.

Equations (104) and (106) depend on an unknown parameter q. However, independently of the precise value of this parameter, the tendency is very clear: the domination of the memory burden takes place latest by the time the

black hole radiates away about half of its mass. That is, the expected upper bound on memory burden time of a black hole is

$$t_{\rm M} \sim S_{\rm BH} R. \tag{107}$$

This is the case for relatively large q. For smaller values of q, the memory burden can dominate sooner. For example, for $q = 2$, this takes place for $\Delta n_\phi \sim \sqrt{S_{\rm BH}}$, i.e., after the time $t_{\rm M} \sim \sqrt{S_{\rm BH}} R$.

Since the intrinsic gaps of the memory and master modes are very different—$m_\phi/m_j \sim 1/(M_{\rm P}R)$—the memory burden effect in black holes is type *II*.

The coefficient of memory efficiency for a black hole can be estimated following the reasoning of [1]. In a black hole of mass $M_{\rm BH}$, the energy difference between the most distant information patterns is $\sim 1/R$. If we would store the same pattern by a nongravitational device of size R on top of a flat space vacuum, then the energy cost would be of order $E_p \sim M_{\rm p} S_{\rm BH}$. The memory-efficiency coefficient at the beginning of evaporation, when black hole is still classical, is therefore

$$\epsilon_{\rm initial} \sim \frac{1}{(M_{\rm P}R) S_{\rm BH}} \sim \frac{1}{S_{\rm BH}^{\frac{3}{2}}}. \tag{108}$$

By the onset of the memory burden effect this becomes

$$\epsilon_{\rm MB} \sim \frac{1}{R M_{\rm P}} \sim \frac{1}{S_{\rm BH}^{\frac{1}{2}}}. \tag{109}$$

In the next section we discuss the mass splitting among the stabilized black hole states.

A. Spread of black hole masses

Since the mass of a stabilized black hole is a function of the memory burden E_p, the prediction is that initially degenerate black holes over time become spread in masses, as schematically given in Fig. 1. This is similar to the evolution of equal mass vacuum bubbles with different values of $N_{\rm G}$.

In order to share with the reader a general sense of scaling, let us analyze an oversimplified toy model in which the memory modes of a black hole are treated as independent qubits with the Hamiltonian (11) with equal intrinsic gaps $m_j = M_{\rm P}$. In this case, $E_p = M_{\rm P} N_{\rm G}$. Correspondingly, the memory burden effect can be measured by the total occupation number of the memory modes $N_{\rm G}$. For M qubits, this number is bounded by $N_{\rm G} \leq M$ and the total number of patterns is given by $n_{\rm st} = 2^M$. This gives the entropy $S_{\rm BH} \sim M$ (more precisely, $S_{\rm BH} = M \ln 2$).

For estimating the spread in this toy model we can use Eq. (103) and take into account that the memory burden effect becomes significant for $\Delta m_\phi \sim 1/R$. We also take into account that for a black hole $m_\phi \sim 1/R$, $m_j \sim M_{\rm P} \sim M$, and $N_\phi \sim M \sim S_{\rm BH}$. However, we keep $N_{\rm G}$ as a free parameter.

Correspondingly, for a black hole of the initial mass $M_{\rm BH}$ and the memory burden $N_{\rm G}$, the relative change in mass by the time of stabilization is

$$\frac{\Delta M_{\rm BH}}{M_{\rm BH}} \sim \left(\frac{S_{\rm BH}}{q(M_{\rm P}R) N_{\rm G}}\right)^{\frac{1}{q-1}} \sim \left(\frac{\sqrt{S_{\rm BH}}}{q N_{\rm G}}\right)^{\frac{1}{q-1}}. \tag{110}$$

One must remember that the above expression is valid as long as

$$N_{\rm G} \geqslant \frac{1}{q}\sqrt{S_{\rm BH}}. \tag{111}$$

This inequality represents a manifestation of the general formula (21) for a black hole. In the opposite case the stabilization is not efficient. Thus, for $N_{\rm G}$ at its lower bound (111), the stabilization takes place at $\Delta M_{\rm BH}/M_{\rm BH} \sim 1$. On the other hand, for $N_{\rm G} \sim S_{\rm BH}$, we recover (104).

Equation (110) tells us that the spread in masses of stabilized remnants is determined by the statistical distribution of $N_{\rm G}$ among the initial black holes. For simplicity of estimate, let us assume that, at the time of formation, the occupation number of the black hole master mode is critical, $n_\phi = N_\phi$. That is, the memory patterns are strictly degenerate. In practice, this is expected to be an extremely good approximation, since the initial black hole is well-described classically up to corrections $\sim 1/N_\phi$.

In such a case, we can assume that the probability distribution of patterns is flat, with no energy bias. Correspondingly, the probability of a pattern with given $N_{\rm G}$ is

$$\mathcal{P}_{N_{\rm G}} = 2^{-M} \frac{M!}{(M - N_{\rm G})! N_{\rm G}!}, \tag{112}$$

which is maximal for $N_{\rm G} = M/2$ with

$$\mathcal{P}_{M/2} \sim \frac{1}{\sqrt{M}}, \tag{113}$$

and the width of $\sqrt{M}/2$. On the other hand, for $N_{\rm G} \ll M$, the probability is exponentially suppressed as

$$\mathcal{P}_{N_{\rm G} \ll M} \sim 2^{-M} \left(\frac{M{\rm e}}{N_{\rm G}}\right)^{N_{\rm G}}, \tag{114}$$

where we dropped polynomial factors for simplicity. Taking into account that the black hole entropy is $S_{\rm BH} \sim M$, the above implies that the probability of forming a black hole with memory burden $N_{\rm G} \ll S_{\rm BH}$ is exponentially small. Thus, it is expected that the most probable black holes are the ones with $N_{\rm G} \sim S_{\rm BH}$.

To summarize, as it is clear from Eq. (110), the change of the black hole mass prior to its stabilization is set by $N_{\rm G}$ as

$$\Delta M_{\rm BH} \propto N_{\rm G}^{-\frac{1}{q-1}}, \tag{115}$$

where the coefficient of proportionality, $M_{\rm BH}(\sqrt{S_{\rm BH}}/q)^{\frac{1}{q-1}}$, is fully determined by the initial mass of a black hole. At the same time, the memory burden $N_{\rm G}$ is determined by the mass only statistically, via (112).

This fact has potentially important observational implications since it predicts a statistical spread of $\Delta M_{\rm BH}$ in addition to the initial mass distribution determined by particularities of a cosmological scenario (see Sec. VII).

B. Fate of a black hole burdened by memory

What happens after a black hole enters the memory burden phase requires a more detailed understanding of the picture. The two possible outcomes were discussed in [3].

The first option is that a new classical (collective) instability sets in and the (former) black hole evolves through it. From our current understanding, it cannot be excluded that due to this instability the remnant can disintegrate via some nonlinear process.

The second (more conservative) option assumes no immediate classical instability. In such a case, the black hole continues to decay via a quantum process. However, due to the memory burden, the process is extremely slow. In [3], the remaining lifetime of a black hole was given as

$$\tau \sim R S_{\rm BH}^{1+k}, \tag{116}$$

where $k > 0$ is an integer. This form follows from the fact that the prolonged lifetime is an analytic function of $S_{\rm BH}$. The analyticity in $S_{\rm BH}$ is enforced by the requirement that the decay rate must be analytic in occupation numbers as well as in gravitational couplings, all of which are set by $S_{\rm BH}$. The case $k = 0$ (zero memory burden) would correspond to a standard extrapolation of Hawking's decay rate.

The value $k > 0$ can be understood from the following argument. In order to continue its decay, the black hole must get rid of the memory burden. That is, the excited memory modes must get deexcited. This can only be done by the scattering processes that involve at least a pair of the memory modes. The memory modes must annihilate into the modes of lower angular momenta in order to match their energies. That is, each mode Y_{lm} must find a partner $Y_{l'm'}$ with very close values of l, m. Such pairs are extremely rare and their annihilation rate is

$$\Gamma \sim \frac{\omega_j^5}{M_{\rm P}^4} \sim \frac{1}{R^5 M_{\rm P}^4}. \tag{117}$$

In terms of the initial entropy, the lifetime translates to

$$\tau \gtrsim R S_{\rm BH}^2. \tag{118}$$

This reinforces Eq. (2), giving $k = 1$ as the most conservative estimate.

C. The effect of species

It is known that black holes provide a link between the number of QFT species $N_{\rm sp}$ and the upper bound on the scale of strong quantum gravity [54–59],

$$M_{\rm sp} = \frac{M_{\rm P}}{\sqrt{N_{\rm sp}}}. \tag{119}$$

The expression is fully nonperturbative and cannot be removed by any resummation of perturbative series. The physical meaning of the scale $M_{\rm sp}$, called "species scale," is that a black hole of size $< 1/M_{\rm sp}$, cannot be treated semiclassically. This can be seen from a number of arguments.

For example, if the standard semiclassical evaporation rate would apply to such a black hole, one would conclude that the black hole would live shorter than its radius, which is absurd.

Similarly, the violation of the bound (119) is excluded by quantum information arguments [57]: a black hole of size $< 1/M_{\rm sp}$, would have the microstate degeneracy, and correspondingly the information storage capacity, exceeding the one of Bekenstein-Hawking entropy (97). In other words, the "species entropy" would exceed the entropy of Bekenstein-Hawking [4].

In general, the increased number of species shortens the standard stage of black hole evaporation by a factor $1/N_{\rm sp}$. This has implication for the memory burden, since the time for reaching this phase is correspondingly shortened [24]:

$$t_{\rm M} \sim S_{\rm BH} R \frac{1}{N_{\rm sp}}. \tag{120}$$

The effect of the species beyond this point is less certain, since due to quantum hair, no universality in decay rates of different species is guaranteed. In other words, the black hole can develop a "species hair" [56]. Therefore, the further decay of the remnant can be biased towards some of the species.

As discussed in [18], already the formula (120) can have important implications for PBH dark matter, as it can shift the masses of memory burdened black holes towards higher values. Furthermore, assuming that decay of the remnant remains approximately democratic in species, the lifetime in memory burden phase will subsequently be shortened by the quantity $\sim 1/N_{\rm sp}$.

V. QUANTUM MEMORY BURDEN VERSUS CLASSICAL EXTREMALITY

It is well known that black holes, as well as solitons, can be stabilized against the quantum decay by classical charges, either Noether or topological. The term "classical" implies that the charge is classically detectable. In other words, the object must carry a classical "hair" with respect to this charge.

In case of a black hole, in the light of "no-hair" theorems [60–62], such are the charges associated with massless gauge fields that can be measured via Gaussian fluxes at infinity.[2] Usually, the amount of charge capable of stabilization is comparable to the mass of a black hole (or a soliton).

We now wish to confront a mechanism of stabilization of an object by a classical hair with the one of a quantum memory burden. For achieving this, we first need to understand the stabilization of a black hole (or a soliton) by a classical charge in a fully quantum language of a microscopic theory.

The first steps in this direction were undertaken in [14]. This microscopic description was further generalized to topological solitons in [37].

In black hole's quantum N portrait [14], a purely gravitational black hole represents a critical coherent state or a condensate of master mode gravitons. The typical energy gaps of these modes are $m_\phi \sim 1/R$ and their mean-occupation number, n_ϕ, is critical, $n_\phi \sim S_{\rm BH}$.

Correspondingly, as in any other system with enhanced information capacity, prior to stabilization, the master modes are the main contributors into the mass of an initially classical black hole,

$$M_{\rm BH} \sim n_\phi m \sim S_{\rm BH}\frac{1}{R}. \tag{121}$$

In this quantum picture, the existence of a classical charge of a black hole means that, on top of the master mode, some other mode carrying this particular charge becomes macroscopically occupied. In other words, a second master mode appears.

For example, the electrically charged Reissner-Nordström black hole contains a macroscopic occupation number of photons. These photons compose a coherent state describing the classical electric field of the black hole. That is, when a black hole carries a classical charge, the "status" of a master mode is shared between the master graviton and some other mode.

Now, as argued in [14], the occupation number of the master graviton sets the upper bound on other occupation numbers. That is, for a black hole the occupation numbers of master modes satisfy the bound,

$$n_{\text{any mode}} \leqslant n_\phi. \tag{122}$$

In this way, the theory [14] provides a quantum explanation of why a black hole charge can never exceed its mass. Notice that this is true for an arbitrary saturon. In particular, (122) is satisfied by saturated vacuum bubbles discussed in Sec. III.

According to [14], a black hole reaches extremality when the occupation number of a certain mode, other than the master graviton, saturates the above bound. In this description, the stability of an extremal Reissner-Nordström black hole can be viewed as the saturation of the bound (122) by the photon constituents of a black hole.

It is intuitively clear [14] as well as evident from computations [70] that in this case the black hole evaporation must stop. The reason is that for maintaining the saturation of the bound (122), a further lowering of the occupation number of the graviton master mode, n_ϕ, must be accompanied by the depletion of the electric field. This is not possible without the emission of the charged quanta. However, the fact that the black hole of size R has an unscreened electric charge to start with implies that in the theory the mass of the lightest charged particle, $m_{\rm e}$, satisfies $m_{\rm e} \gg 1/R$. In the opposite case, the charge would be screened by the Schwinger effect.

Correspondingly, the quantum emission of electric charge is exponentially suppressed, since such a process requires a rescattering of many soft constituent quanta (of energies $\sim 1/R$) into a quantum of energy $m_{\rm e} \gg 1/R$. The transition rate of such processes is bounded from above by $e^{-m_{\rm e}R}$, as indicated by a general argument given in [4]. This is confirmed by explicit computations of corresponding multiparticle processes [70]. The suppression of the transitions many $\to$ few can also be extracted from explicit computations of graviton scattering processes [71,72]. The analogous suppression is exhibited by scalar theories [73–80].

Thus, the characteristics of black hole stabilization by a classical charge is the existence of a long-range classical hair with respect to that charge. At the same time, the quantum information pattern carried by the black hole plays no role. For example, the extremal black holes of the same electric charge and mass can carry information patterns of very different content.

In contrast, when a black hole is stabilized by a quantum memory burden, no classical charge associated with a long-range gauge field is required. Of course, a macroscopic "hair" emerges in form of a memory burden parameter, $N_{\rm G}$. This parameter is in principle measurable by a scattering experiment, but there is no inconsistency with the no-hair properties: since the memory-burdened black hole is a quantum object, it has no reason to respect classical no-hair theorems. Therefore, unlike classical extremal case, there is

[2]The seeming exceptions, such as a classical skyrmion hair [63–65], have been shown [66,67] to be equivalent to Aharonov-Bohm type hair under a discrete gauge symmetry [68,69].

no specific gauge charge or a long-range Gaussian flux associated with the quantity N_G.

The difference between the two mechanisms is also clear from the fact that the decay of a memory-burdened black hole is not suppressed exponentially but only slows down as a power law (2).

Interestingly, the solitons stabilized by the memory burden unify both features. The main reason is the existence of two types of microstates discussed above.

The first category of microstates have equal N_G but are distinguished by the relative $SU(N)$ transformations. These remain exactly degenerate even after the memory burden sets in. The microstates belonging to the second category are distinguished by values of N_G. The energies of such microstates get split after stabilization.

Both sets of microstates have counterparts in a black hole. As discussed, the microstates of a black hole correspond to degeneracy of patterns obtained by occupation numbers of different memory modes Y_{lm}. Among these states, there exist both categories: with equal and distinct memory burdens. As time elapses, the level splitting develops according to the memory burdens they carry, as given in Fig. 1.

Another example of a classical "charge" that can stabilize a black hole against quantum decay is the angular momentum. The similar case in solitons reveals a certain interesting peculiarity.

The stationary $SU(N)$ bubble with nonzero spin is obtained via giving the winding number n to the Goldstone mode [11]. Basically, the matrix U in (74) is replaced by

$$U = e^{i(t\omega + n\varphi/\sqrt{2})\frac{\omega_j}{\omega}T^j}, \tag{123}$$

where φ is the polar angle and the factor $\sqrt{2}$ is added to ensure the phase continuity.

The winding of the Goldstone phase produces the vorticity and, simultaneously, the angular momentum,

$$J = \int \mathrm{d}^3 x\, T_{0\varphi} = n\, N_G = n\, Q, \tag{124}$$

where $T_{\mu\nu}$ is the energy momentum tensor.

The fact that the winding number n induces the spin given by (124) has been known for Q balls with $U(1)$ charge [47,48,81]. The remarkable thing about the saturated $SU(N)$ vacuum bubbles is that Eq. (124), describing the relation between the maximal spin and the entropy, is strikingly similar to the one satisfied by a black hole [11],

$$J_{\max} = S. \tag{125}$$

A saturon vacuum bubble of $SU(N)$, which has entropy

$$S = N_G, \tag{126}$$

reproduces the relation (125) due to the limited vorticity, $n \sim 1$, that it can sustain. Attaining a higher spin would require a larger vorticity, $n \gg 1$, which would increase the mass and the size of the bubble, thereby making it undersaturated.

Note that the relation (125) is shared by other saturons. For example, it is automatic in saturated baryons in QCD with a large number of colors and flavors [5].

The same relation is shown [82] to be shared by a saturated version of a spinning cosmic string loop (a so-called vorton [83]).

To summarize, the saturon bubbles of maximal spin exhibit the exact same relation between spin and entropy as the extremal spinning black holes. At the same time, in extremal saturon bubbles this relation reveals an explicit microscopic meaning in terms of vorticity.

Notice also that vorticity gives a topological meaning to the quantum stability of the extremal bubble [11]. Indeed, the decay of a bubble via the particle emission is blocked because of conservation of the topological winding number. The decay is only possible if the entire vortex is ejected via a quantum tunneling, which is an exponentially suppressed process.

In this sense, the extremal spin represents another form of a "classical" memory burden. As in the case of the burden induced by a pure $SU(N)$ charge, the burden induced by the spin is due to a critical occupation number N_G of a Goldstone/memory mode. For a saturon bubble, $\omega \sim m$, this memory mode becomes an additional master mode. The difference from nonspinning case is that the macroscopically occupied memory mode has a nonzero angular momentum.

This analogy is fully extended to black holes if we conjecture that a spinning black hole corresponds to the one in which a mode of a particular angular harmonic Y_{lm} is macroscopically occupied. In this light, it is interesting to discuss a conjecture of [11] stating that the extremal spin in a black hole is accompanied by vorticity, similarly to the case of a spinning saturon bubble. Again, as in the case of a bubble, the vorticity gives a topological explanation to the quantum stability of the extremal black hole. In the case of the spin, similarly to other classical charges, the extremal black hole does carry a classical hair in form of the angular momentum.

To summarize, there exist fundamental differences between the black holes stabilized via classical charges and the ones stabilized by a quantum memory burden effect. One obvious difference is that the classical extremality is necessarily accompanied by a long-range classical gauge hair.

This is not the case for a black hole stabilized by the memory burden effect. Instead, for a memory-burdened black hole, the hair is short range and carries no Gaussian flux at infinity.

More importantly, a memory-burdened black hole carries a significant quantum hair. The significance is measured by the fact that the energy of the quantum information pattern is comparable to the mass of the remnant.

Such a remnant is neither a black hole nor classical, and, therefore, is not constrained by classical no-hair theorems. Although macroscopic, it nevertheless is a quantum entity. This "macroquantumness" is a feature of black holes [16] as well as of other saturons [4].

The above important difference between the quantum memory burdened and (quasi)extremal black holes must be taken into account when applying such mechanisms of stabilization to light PBH dark matter. In particular, if the naive semiclassical timescale required for approaching extremality is longer than the memory burden time $t_{\rm M}$, the latter effect becomes the dominant one and must be taken into account.

In addition to differences at a fundamental level, this will have observational consequences. For example, the memory-burdened PBH dark matter [3,17–21] will be subjected to the mass spread discussed in the present paper. This spread is absent for PBHs stabilized by extremality within the validity of semiclassical regimes, such as discussed in [84] (and references therein).

The fundamental difference between the prolongations of a black hole lifetime due to a classical hair versus the quantum memory burden effect, extends beyond the ordinary black holes. The example is provided by a black hole smaller than the compactification radius in the framework of large extra dimensions [85].

Such a black hole is a solution of Einstein's equations in high-dimensional gravity and its radius and temperature are defined by the fundamental Planck mass, $M_{\rm F}$, which is suppressed relative to the four-dimensional one by the volume of extra space [85]:

$$M_{\rm F} = \frac{M_{\rm P}}{\sqrt{V_{\rm extra}}}. \tag{127}$$

Correspondingly, the high-dimensional black holes are colder relative to wouldbe four-dimensional black holes of the same mass. It was proposed in [86,87] that such black holes can serve as dark matter.

Let us confront the Kaluza-Klein (KK) hair of young high-dimensional black holes with the memory burden effect. Of course, the question arises solely from the point of view of a four-dimensional observer, since from high-dimensional perspective these are usual classical black holes.

From four-dimensional perspective, the decay of high-dimensional black holes can be understood in terms of species. First, as discussed in [54], Eq. (127) can be viewed as a particular case of (119), with the role of particle species played by KK gravitons and the role of the four-dimensional species scale assumed by the fundamental Planck mass $M_{\rm sp} = M_{\rm F}$.

When evaluating the evaporation rate, we must take into account that the black hole is smaller than the compactification radius, correspondingly, it develops the species hair [56]. That is, the black hole sources a tower of massive KK gravitons to which it also evaporates. The evaporation into many KK species is equivalent to the emission of a single high-dimensional graviton [58].

Therefore, the evaporation of a young black hole is well-described semiclassically through a high-dimensional Hawking process. From the point of view of a four-dimensional observer it is an object that caries a classical species hair [56] under KK gravitons. Such a classical hair is fundamentally different from the quantum memory burden that sets in at a later stage.

This is already evident from the fact that quantum memory burden will be experienced by a high-dimensional black hole after it gets sufficiently "old." Extrapolating our results, we can say that this will happen the latest by half-decay. Therefore, for a high-dimensional PBH, the quantum memory burden effect must be taken into account in the same way as for ordinary Einsteinian black holes.

VI. NUMERICAL ANALYSIS: STABILIZATION OF SOLITONS

We summarize here our numerical findings. We focus on the dynamics of underburdened solitons, whose evolution, as discussed in Sec. V, offers analogy with evaporating black holes that are stabilized by their quantum memory.

The idea is to start with a vacuum bubble, with the value of the charge $N_{\rm G}$ given by (92). As discussed in Sec. III B, this amount of charge is insufficient for an immediate stabilization. In particular, for such a bubble the energy of the memory pattern is negligible as compared to the energy of the master mode (92), which constitutes the main source of the energy.

Such a bubble oscillates, emitting energy and correspondingly shrinking in size. We map this stage of evolution on the one of a black hole before entering the memory burden phase.

The decay process of the bubble continues up until the Goldstone charge fulfils the condition (90). Simultaneously, the energy of the memory pattern catches up with the energy of the master mode (86). Correspondingly, the bubble is stabilized by the burden of memory. At this point, the bubble becomes a stationary Q ball.

Let us denote the reference stationary Q-ball charge by $Q_{\rm s} = N_{\rm G}$ and its frequency by $\omega_{\rm s}$. We then vary the initial charge by changing the frequency of constituents, while keeping the profile fixed, to the following values

(1) $\omega = 3\omega_{\rm s}/4$, $Q = 3Q_{\rm s}/4$.
(2) $\omega = \omega_{\rm s}/2$, $Q = Q_{\rm s}/2$.
(3) $\omega = \omega_{\rm s}/4$, $Q = Q_{\rm s}/4$.
(4) $\omega = 0$, $Q = 0$.

resulting in underburdened configurations of different $N_{\rm G}$ [therefore, not related by a $SU(N)$ transformation] in the regime (92) and (91).

Our numerical analysis supports the analytical discussion of the previous sections. Namely, the bubbles of different initial charges—but of similar energies—while

they have analogous dynamics at initial times, are stabilized towards Q-ball configurations of different masses.

The statement holds true for all regimes analyzed in our study—regardless of other details such as the winding number, the inclusion of new interactions and the thickness of the bubble wall. This shows that the mechanism of stabilization by memory is a general consequence of the high-memory storage capacity of the object and is only secondarily affected by other features, such as, for example, saturation or vorticity. Consequently, this further supports the prediction of Sec. III C that an analogous mass splitting is expected in the asymptotic distribution of black holes of equal initial masses but different memory burdens.

The rest of this section is dedicated to showing how the above statement comes about. For numerical simplicity, we focus on the $SU(4)$ symmetric case. Unless otherwise stated, we fix $\alpha = m = 1$ in units of f and choose $\omega = 0.3m$. Since we are interested in the winding $n = 0$ and $n = 1$ cases, a $(2+1)$-dimensional analysis is sufficient. Furthermore, absorbing boundary conditions are adopted. Finally, some of the simulation visuals can be found at the following [30].

A. Winding $n = 0$ case

The energy density evolution is shown in Fig. 2. For $Q = 3Q_s/4$ (first panel), the system is close to the stationary case, and therefore has a significant burden. In fact, the bubble starts collapsing, but the information (charge) stored within immediately backreacts on the dynamics. This, in turn, results in an oscillatory behavior analogous to what was already observed in [10]. The reason the bubble does not relax to its stationary configuration is energetic. Simply, the excitations are smaller than the mass gap outside of the configuration. As a consequence, (almost) no charge is emitted and the information is retained within the bubble. This is a manifestation of the existence of the information horizon [10]. The notion becomes exact in the semiclassical limit which corresponds to large N.

This can be seen explicitly in the third column of Fig. 2 where the integrated energy and charge densities are shown as functions of time (the integrated charge, corresponding to the blue line, is obscured by the cyan curve of the case $Q = Q_s/2$).

An analogous situation is observed in the second panel of Fig. 2. Since in this case the initial charge is smaller —$Q = Q_s/2$—the resulting oscillations are more pronounced. Still, the burden forbids the collapse, and the energy gap ensures that almost no charge is emitted. The oscillatory frequency of the profile in both cases is roughly given by R^{-1} as it can be qualitatively seen from the plot. A perturbative analysis of the system energy would inform us of this fact, as already shown in [10].

In the first panel of the second row, for $Q = Q_s/4$, the energy of the collapse is sufficient for overcoming the mass

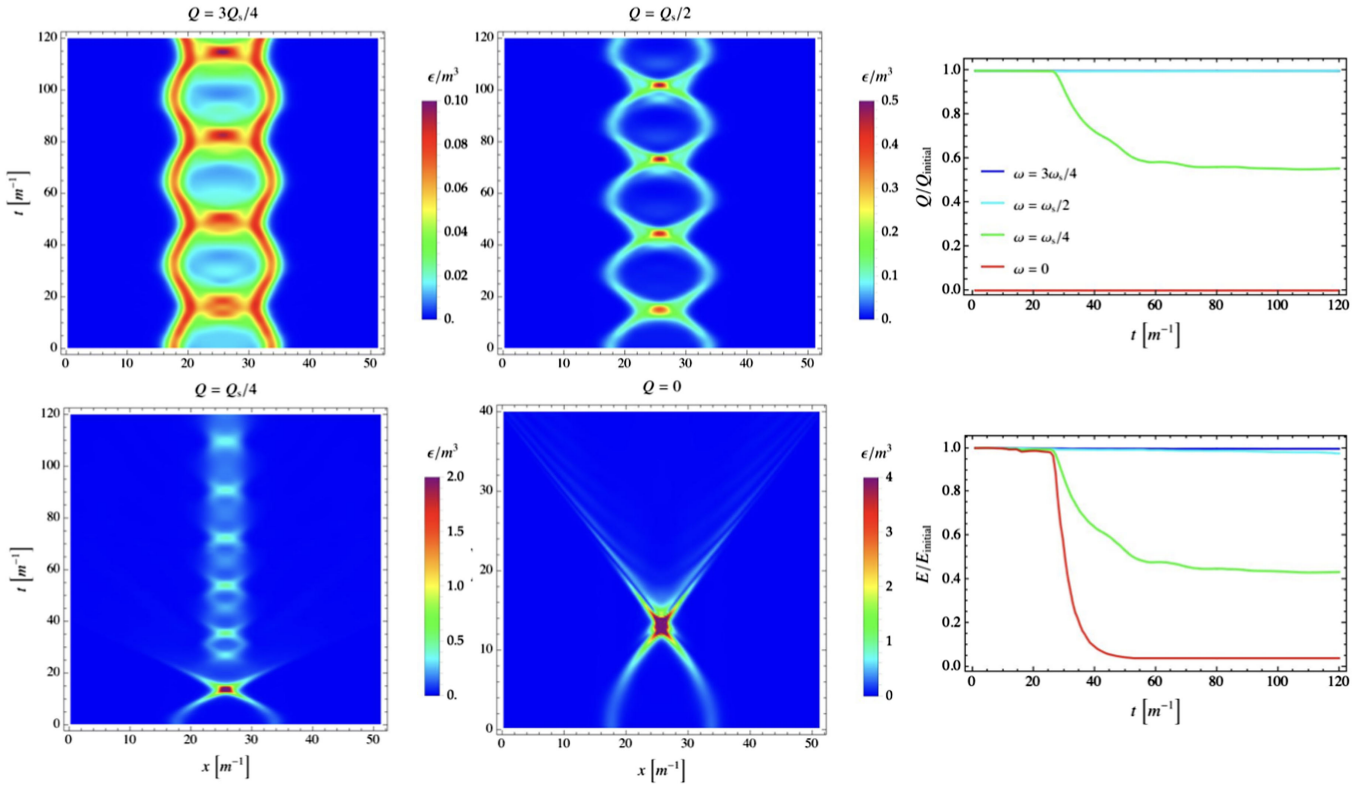

FIG. 2. Energy density evolution for different initial charges and winding $n = 0$. The third column shows the integrated charge and energy as functions of time.

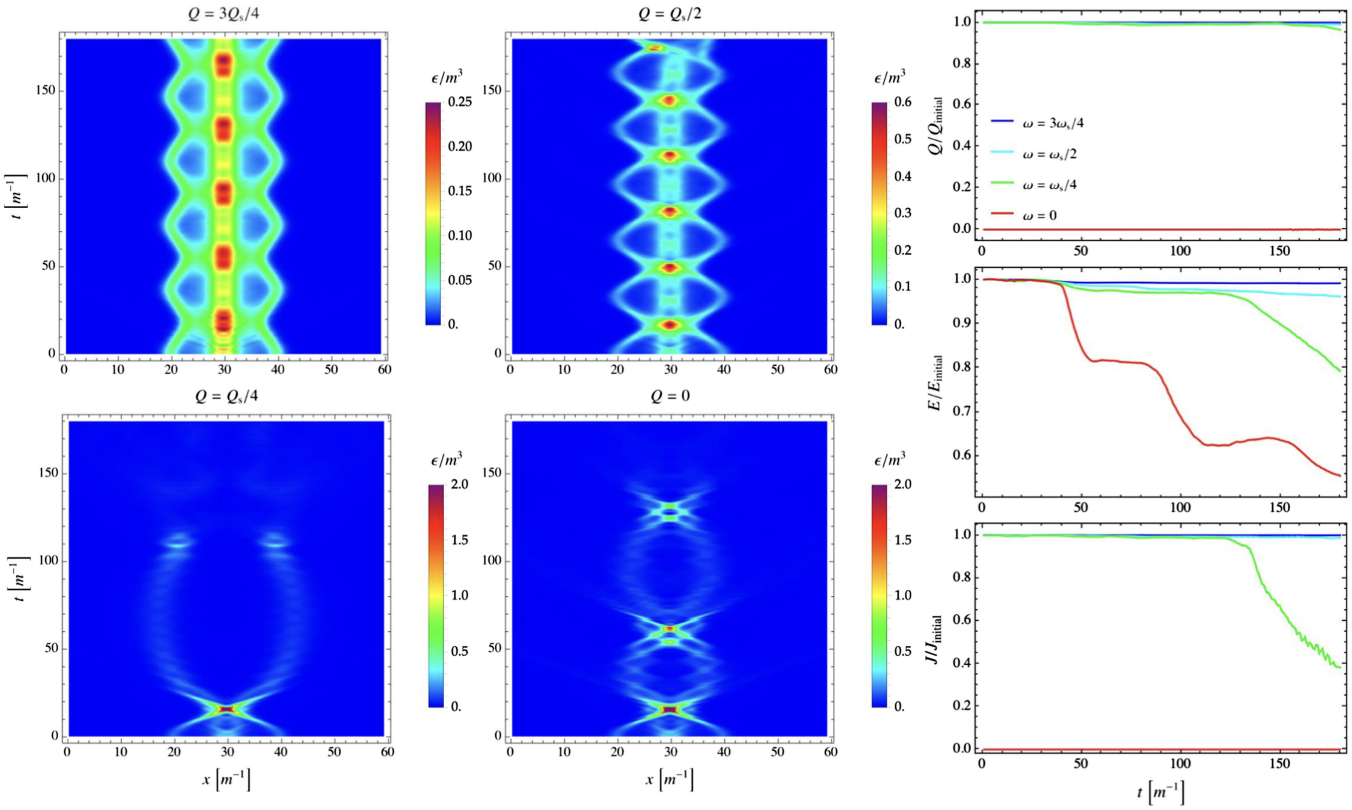

FIG. 3. Energy density evolution for different initial charges for winding number $n = 1$. The third column shows the integrated charge and energy and angular momentum as functions of time.

gap outside of the Q ball. As a consequence, charge is emitted and part of the information is lost in the first oscillation as it can be seen in Fig. 2. At later stages, the pulsation energy becomes insufficient for exciting new quanta, resulting in a stationary configuration with smaller charge and radius. For analysis of such excitations in $U(1)$ symmetric Q balls, see, e.g., [88].

Finally, in the zero charge no burden is present to stop the collapse. The system is effectively a bubble interpolating between two degenerate vacua. Therefore, the collapse due to the surface tension takes place within one oscillation and is rather violent. However, for smaller values of coupling, the oscillation can last longer.

B. Winding $n = 1$ case

Memory burden has an analogous stabilizing impact on underburdened bubbles endowed with vorticity characterized by winding number $n = 1$. We refer the reader to [89] for the numerical construction of the stationary solution.

As discussed in Sec. V, vorticity is realized in terms of a macroscopic occupation number of Goldstones under the ansatz (123), leading to nonvanishing angular momentum according to (124).

Since saturated bubbles with vorticity and black holes obey the same maximal-spin bound—cf., (125)—one might be tempted to map underburdened bubbles with vorticity on evaporating black holes dynamically approaching extremality. Of course, within the semiclassical picture, whether or not a black hole evolves towards such point, is determined by the particle spectrum participating in the emission [90]. However, the semiclassical analysis does not take into account the memory burden effect which invalidates it. This must be kept in mind when mapping the quantum evolution of a black hole on the dynamics of underburdened bubble in our numerical analysis.

The first panel in Fig. 3 shows the evolution of energy as a function of time for the case $Q = 3Q_s/4$. Although the simulation is performed in two spatial dimension, for illustrative purposes, we slice here along the x coordinate, fixing y along the center of the vortex. The situation is similar to the $n = 0$ case with similar initial charge. Notice that in this case the energy of the vortex in the central region oscillates together with the pulsating radius of the configuration. The period of pulsation also here is of order $R^{-1} - R$ being the radius of the stationary configuration (and therefore, also the initial radius at the simulation time). As expected, the bubble is stabilized by the conserved charge and the angular momentum in its interior—see third column of Fig. 3.

A similar behavior is observed in the second panel for $Q = Q_s/2$. Indeed here the pulsations are more pronounced due to the larger initial off balance between

memory and master mode energy. Concomitantly, a mild emission of energy and charge is observed through the initial collapse. Notice that at the end of the simulation, at large time, the axial symmetry is broken. Consequently, instability mode grows in time, eventually leading to the emission of the vortex. The numerical duration of the simulation is insufficient to capture the impact of this phenomenon on the integrated quantities in Fig. 3. However, we have already characterized it in [12] when studying soliton mergers. Therein, we noted that a vortex localized in the merged configuration is unstable, therefore resulting in its eventual ejection. Examples of such dynamics can be found at the following [91,92].

A different behavior is observed in the first panel of the second row for $Q = Q_s/4$. In this case, the first collapse is extremely violent, and one might naively expect the features analogous to the case $n = 0$. Instead, only a negligible charge is emitted by the configuration, which is localized in a large ring around its center. The ring is, effectively, a slowly rotating (quasi)oscillon. Eventually, due to the broken axial symmetry, for $t \gtrsim 120m^{-1}$, the system fragments into smaller Q balls [a phenomenon known in the case of $U(1)$-symmetric Q balls, see, e.g., [93,94]], which cannot be visualized due to the y cut of the plane performed in the figure. The phase keeps rotating between the fragmented Q balls due to the angular momentum of the configuration. Correspondingly, significant amount of energy and angular momentum are expelled from the configuration, as can be visualized at the following [30] and Fig. 3 show.

Analogous dynamics, eventually leading to fragmentation is observed also for vanishing charge (red line). Energy is discretely emitted from the configuration as the outer wall of the bubble squeezes the central vortex. These correspond to the three observed pulses in the fourth panel of Fig. 3. Characterization of both phenomena of fragmentation, as well as vortex ejection, are beyond the scope of this work.

C. Derivative interaction case

In order to make the analogy between bubbles and black holes maximally transparent, and to allow for a significant relaxation of the configuration pulsations, we further extend the system by derivatively coupling the soliton field to a $SU(N)$-singlet scalar χ via the Lagrangian,

$$\mathcal{L} \supset \frac{1}{2}\partial_\mu\chi\partial^\mu\chi + \frac{g}{2}\chi \mathrm{Tr}(\partial_\mu\Phi)(\partial^\mu\Phi) - \frac{\lambda}{4}\chi^4. \quad (128)$$

The above interaction term is sensitive only to the master mode of the saturon, while leaving the charge unaffected. The mechanism of stabilization by memory proceeds similarly to the previous cases.

In units of m, the couplings are $g \simeq 0.5$ and $\lambda \simeq 0.15$ and we further initialize χ to be vanishing. The resulting energy density evolution, adopting analogous initial conditions to the cases discussed in the previous subsection, are displayed in Fig. 4. The top row shows the dynamics for the case of winding number $n = 0$, while the bottom corresponds to the case with vorticity. The cases with charge $Q = 3Q_s/4$ (first column) and $Q = Q_s/2$ (second column) are sufficient for our discussion.

Although χ is massless, a full relaxation is not possible. In fact, the derivative interaction sources a tadpole for χ, which therefore localizes on the bubble support. A quartic coupling has been added in (128), in order to tame the growth of χ. This setup effectively generates a local mass gap for χ of magnitude $\sim(\sqrt{g}\lambda\omega^2 f^2)^{1/3}$. This backreacts on the capacity of the system to fully relax to a stationary configuration, and constitutes the main reason we observe oscillations—although much less pronounced—at late times. This is in stark contrast to the case without singlet χ of the previous subsection cf., Figs. 2 and 3, in which the bubble simply pulsates with almost constant frequency and amplitude.

The integrated energy confirms this behavior as shown in the third column of Fig. 4. Clearly, significantly more energy is emitted in the case of initial charge $Q = Q_s/2$ (red lines) as this is further away from being stationary and, therefore, has more energy available for the emission. In general, for $n = 1$ (dashed lines), the energy damping is both faster and more efficient, due to the extra gradient energy of the bubble background around the vortex region. Nevertheless, charge is well conserved—within 1%—throughout the simulation time. This is expected given the nature of the coupling, not sensitive to the flavor of the bubble.

Compared to the case without χ, the charge and the energy of the bubble are seen to be significantly more oscillatory. Notice that the derivative interaction leads to a redefinition of charge by a factor $1 + g\chi$. In fact, the oscillatory behavior is seen in correspondence of χ oscillations on the bubble support. The effect is larger at the beginning of the simulation since the χ field is very far from equilibrium and this leads to violent oscillations, modestly challenging the capabilities of our numerical implementation (as expected, given that we are dealing with a derivative interaction term).[3]

[3]In order to be exactly charge and energy conserving, an indirect inversion method should be used when computing the time-evolution involving a matrix of both ϕ and χ at each lattice point. This is not very efficient, as a huge matrix should be inverted at once, leading to a significant restriction on the lattice dimension. Instead, we adopt a direct method, based on finite difference, and compute each $t+1$ component of the field restricting to neighboring points from time slices at t and $t-1$, t being the index characterizing the step number. In practice, an exact method for the ϕ field evolution is used, evaluating all time derivatives with central scheme at the time slice t and using it to obtain the $t+1$ component. However, then to update the χ field it becomes necessary to use a backward derivative for source term proportional to g. This induces an error in our algorithm dependent on the time step size which, we verified, reflects—partly—the amplitudes of the peaks in the first panel of the third column of Fig. 4.

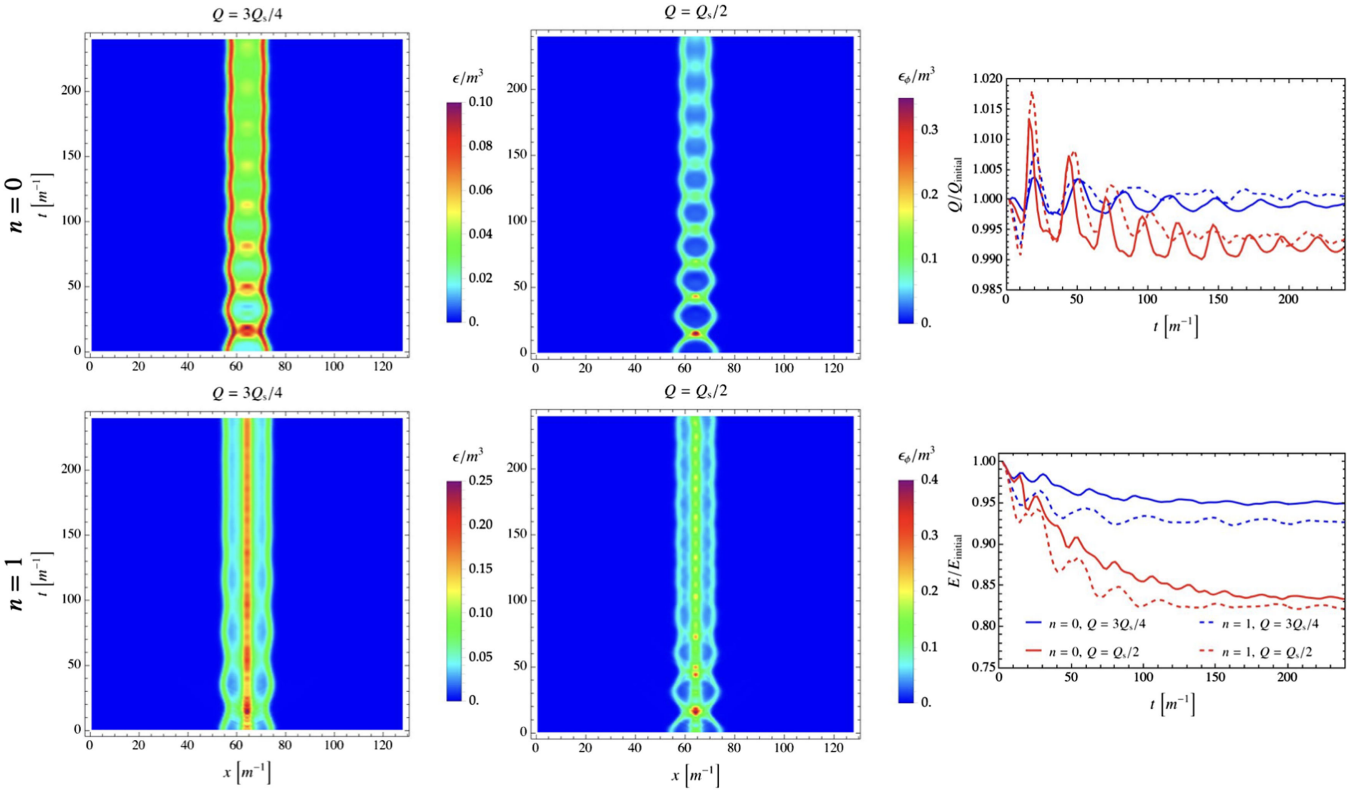

FIG. 4. Energy density evolution for different initial charges for winding number $n = 0$ (top row) and $n = 1$ (bottom row) for nonvanishing interaction with derivatively coupled singlet χ. Third column shows the integrated charge and energy as functions of time.

Finally, analogously to the case of the previous subsection, in the last panel we can observe the onset of the vortex ejection phenomenon towards the final stage of the evolution.

D. Thick-wall regime

So far, our numerical analysis focused on bubbles in the thin-wall regime. Although such bubbles are undersaturated in terms of the bound (4), they nevertheless represent the systems of enhanced capacity of information storage. This is fully sufficient for understanding the key features of the memory burden effect and mapping it on black holes. In fact, the thin-wall bubbles are very well suited for capturing the type-*II* nature of the black hole memory burden effect.

On the other hand, in the thick-wall regime the bubble/Q-ball represents a saturon [see discussion around Eq. (69)]. This has advantage of reproducing the feature of a black hole in terms of the area-law scaling of entropy (4). Therefore, we shall also study this case.

As we will see, at a qualitative level, statements analogous to the ones of the previous subsection hold also in this regime, providing further evidence for the generality of the stabilization by the burden of memory. However, there are some quantitative differences, since the memory burden effect in thick-wall bubbles is of type *I*.

The two panels in the third column of Fig. 5 show the energy and the charge of the configuration as functions of time for the four cases of underburdened bubbles, corresponding to the four different colors and compare the cases without (continuous) and with (dashed line) the derivatively coupled singlet χ. For simplicity, we focus on the case of zero winding. Moreover, we chose $\omega_s = 0.8m$, while keeping other parameters unchanged.

One notable feature in the thick wall regime is that the constituents within the bubble have larger frequency. Therefore, it is easier to excite modes above the asymptotic mass gap, as compared to thin-wall case. This, in turn, leads to a progressively larger relative emission of charged particles as the initial charge of the configuration decreases. This is due to the fact that the system is in the type-*I* regime, which, for larger ω, has a worse storing efficiency—see Eq. (89).

Remarkably, charge emission seems alleviated in presence of χ field, as another channel becomes available for relaxation, allowing the system to reach equilibrium while retaining information. On the other hand, a significant amount of pulsation energy is depleted due to the presence of the singlet.

A further comment related to the behavior of the system at small and vanishing charge (green and red line, respectively) is due. In this case, the system does not collapse, as opposed to the thin wall scenario. Instead, only a small

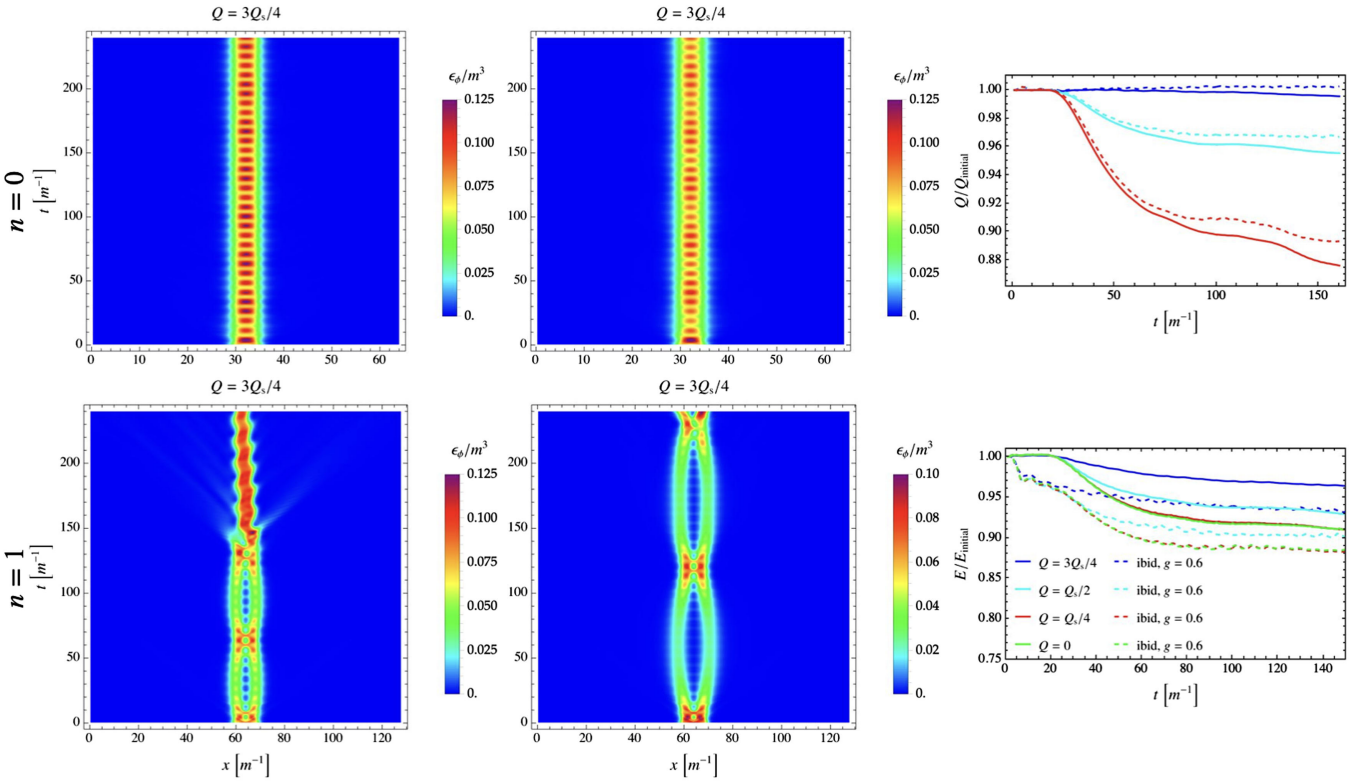

FIG. 5. Energy density evolution for different initial charges for winding number $n = 0$ (top row) and $n = 1$ (bottom row) for vanishing (left column) and nonvanishing (central-column) interaction with derivatively coupled singlet χ. The third column shows energy and charge evolution as functions of time for $n = 0$ winding.

fraction of the initial energy is emitted; the reason being that the "oscillon" configuration is not sufficiently excited to produce asymptotic quanta. This basically results in stationary configurations. Equally stated, the oscillation frequency of the oscillon is smaller than the asymptotic mass gap.

For completeness, we report in Fig. 5 also the energy density evolution of underburdened bubbles in the thick-wall regime for the winding numbers $n = 0$ (first row) and $n = 1$ (bottom row). In the left column the singlet coupling is $g = 0$, while in the central column $g = 0.6$. In the $n = 1$ case, we can observe a marginal energetic emission due to the presence of the singlet χ channel of about 5%–10% of its total energy.

Noticeably, in the third panel, a vortex ejection takes place at $t \simeq 150m^{-1}$. Correspondingly, the configuration looses about 40% (30%) of its initial energy (charge). Moreover, since the vortex is responsible for the spin, its ejection causes a drop of about 90% of the total angular momentum (we, once gain, refer the reader to [12] for a detailed discussion of this phenomenon). In the case of derivative interaction (central panel) the ejection takes place later, towards the end of the simulation time, indicating that the derivative coupling can stabilize the vortex within the Q-ball support.

VII. IMPLICATIONS AND OUTLOOK

The goal of the present paper was to further investigate the physical nature and the extent of universality of the memory burden phenomenon [1,3]. After introducing the essence and generic features of the phenomenon, we have studied its manifestations in solitons building up on the previous work [10].

We have established a close correspondence with the expected features of the memory burden phenomenon in black holes. In this analysis, we took a double approach. On one hand, following [1,3], we have modeled the memory burden effect in black holes relying exclusively on their well-established features. These features unambiguously place black holes in the category of objects of enhanced capacity of information storage susceptible to the memory burden effect.

On the other hand, we used a microscopic theory of black hole's quantum N portrait [14,15] as the reference point for the consistency checks of our results.

The emerging picture speaks in favor of close similarities between black holes and other objects of enhanced capacity of information storage, such as the solitonic saturons [4–12].

We have confronted the stabilization via memory burden with the stabilization by means of the classical hair and

outlined the fundamental differences between the two mechanisms.

We have predicted that the memory burden effect induces the mass splitting between initially degenerate black holes according to differences in their information patterns.

We have performed numerical analysis for various regimes of the solitonic memory burden, with or without the topological winding numbers. The results of these numerical simulations fully confirm our analytic conclusions.

Let us now briefly go over some implications of the memory burden effect and the future prospects.

A. New dark matter window for PBH

As put forward in [3], one immediate implication for black hole stabilization by the memory burden effect is the opening of a new window for PBH dark matter in the range of masses below $\sim 10^{14}$ g. The idea of PBH goes back to [95–97], and the proposal of PBH composition of dark matter is also old [98] (for a review, see [99]). However, in the standard treatment, in which one extrapolates the Hawking regime till the very end of black hole existence, the PBH of masses below $\sim 10^{14}$ g were assumed to be excluded from dark matter, since they were expected not to survive till the current epoch.

The understanding that black holes undergo the memory burden effect [1] and can get stabilized by it [3] drastically changes the standard view. PBHs in the wide range of masses below 10^{14} g can now account for the entirety of dark matter. The proof-of-concept type examples of light PBHs (e.g., with masses $\sim 10^8$ g) that satisfy all the known constraints, were originally given in [3].

Furthermore, the possibility of dark matter in the form of PBHs stabilized by memory burden in the mass range above $\sim 10^4$ g [corresponding to most conservative value $k = 1$ in (116)] was discussed in [17]. This paper proposes an explicit cosmological mechanism for the formation of such PBHs in the right abundance.

A further analysis of various constraints on light ($\lesssim 10^4$ g) PBH dark matter stabilized by memory burden was offered in two recent papers [18,19]. In particular, it was shown that PBHs that enter the memory burden phase prior to BBN epoch, are unconstrained from BBN and CMB. For the most conservative estimate of the post-memory-burden lifetime, corresponding to $k = 1$ in (2), these are PBHs with masses below 10^9 g. Such PBHs can easily compose the entirety of dark matter. Further implications of the memory burden effect for PBHs can be found in [20,21] (see [100] for some future prospects).

The analysis of the present paper predicts a spread in PBH dark matter masses, regardless of their production mechanism. This is due to the mass splitting of the remnants evolving from initially degenerate black hole states, as shown in Eq. (110) and schematically described by Fig. 1.

Let us consider a black hole, formed at time t_f with initial mass $M_{BH}(t_f)$, which entered the memory burden phase around some time t_M, prior to today's Hubble time. For definiteness, let us assume that the subsequent change of the mass is negligible. For instance, this will be the case for $k > 0$ and $M_{BH}(t_f) \gtrsim 10^4$ g.

However, the mass of PBH at stabilization is determined by the memory burden that it carries (115). To the leading order, the burden is controlled by the occupation number of the memory modes, N_G. As we have discussed, statistically, the most probable value of this number is of the order of the PBH initial entropy S_{BH}. The probability of forming a black hole with memory pattern $N_G \ll S_{BH}$ is exponentially small. This implies that most of the PBHs that we observe today as dark matter carry the memory burdens of order the initial entropy $N_G \sim S_{BH}$, with the statistical spread given by (112). This translates as the corresponding spread in PBH masses via (115).

In particular, PBHs of masses $M_{BH} \lesssim 10^{14}$ g are subjected to this spread. Notice that in case of existence of a large number of hidden particle species, the time t_M gets shortened as (120) [24]. Due to this, the memory burden can affect much heavier PBH dark matter [18]. Correspondingly, the prediction of the mass spread will extend to such black holes.

Notice that the spread is predicted even if the production of PBHs is sharply peaked at a particular mass.

A schematic representation of this effect is provided in Fig. 6, where the fraction of PBH energy density as dark

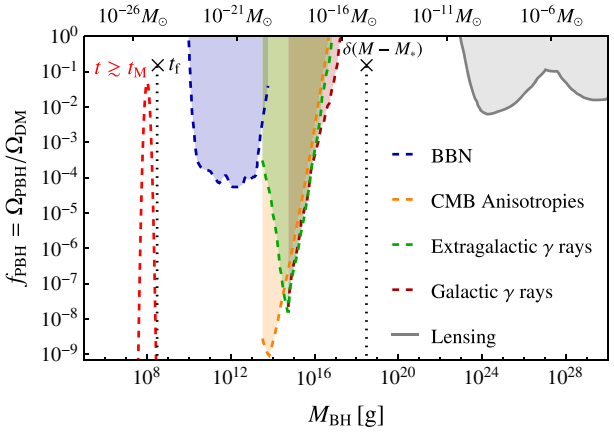

FIG. 6. f_{PBH} as a function of M_{BH}. Shaded areas represent existing constraints—we refer the reader to [19,101,102] for an accurate description. The ones on the left follows from Hawking evaporation and are, therefore, only mildly affected by the most conservative estimates of memory burden effect, $k = 1$ [see (2)]. Dotted lines represent the monochromatic distribution at formation time t_f. PBHs lighter than 10^{14} g (ignoring corrections due to large number of species) are affected by the burden over cosmological times, resulting in a smearing of the distribution, with spread of order M_*, for $t \gtrsim t_M$. The qualitative spread is schematically shown by the red-dashed line.

matter, $f_{\rm PBH}$, is shown as a function of the PBH mass, $M_{\rm BH}$. The shaded areas denote the existing bounds. To explicate our point, at formation time, $t_{\rm f}$, we consider two monochromatic distributions peaked at $M_* \sim 10^{18}$ g and 10^8 g.

The former is in the currently unconstrained asteroid mass window where PBHs can constitute an $\mathcal{O}(1)$ fraction of dark matter. Ignoring a possibility of large number of hidden particle species (120), these objects are unaffected by their memory over the cosmological timescales.

The latter (lighter) PBH distribution, instead, lies in the new mass window opened by the memory burden effect. At late times, $t \gtrsim t_{\rm M}$, PBHs are stabilized by their memory. Consequently, the distribution—pictorially represented by the red-dashed line—develops a spread of order M_* according to (115).

Of course, the quantitative confrontation of the model-independent spread (115) with the model-dependent one coming from particularities of a production mechanism can only be performed within a specific cosmological scenario providing such a mechanism. For example, the mechanism of [17] is based on black hole production due to collapse of confining strings connecting the heavy quarks and antiquarks. Strings are produced and stretched during inflation. After reentering the Hubble patch, the string tension pulls the quark and antiquark towards each other, colliding them and forming a PBH (see [103] for a numerical simulation of the dynamics).

This mechanism has certain intrinsic spread of PBH masses, due to the factors such as the duration of inflation. The memory burden imposes an additional spread (115), due to a statistical distribution of the initial memory burden of the type (112).

We must note that possibility of black hole stabilization at macroscopic size due to quantum backreaction has been suggested previously in [28]. Even if such additional mechanisms are realized, the memory burden effect must be taken into account regardless, since it represents a generic physical mechanism of stabilization. Most importantly, this phenomenon is universal for systems of enhanced information capacity and independent on particularities of a microscopic picture [1,3].[4]

B. Implications for inflationary cosmology

As proposed in [22,24], the memory burden effect can be applicable to cosmological spacetimes such as de Sitter or inflation. This is due to the fact that, just like a black hole, a de Sitter Hubble patch of radius R represents a system of enhanced information capacity. The evidence for this is provided by Gibbons-Hawking entropy of de Sitter space $S_{\rm GH}$ [23], which is very similar to the Bekenstein-Hawking entropy of a black hole (97).

[4]In a separate context, the memory burden effect can play an important role in dark matter composed of nongravitational saturons [104].

In fact, treated as a coherent state of gravitons constructed on top of the Minkowski vacuum, the quantum portrait of de Sitter [16,25,26,105] shares some key features with a similar portrait of a black hole [14]. For example, the Gibbons-Hawking radiation is a result of the quantum depletion of the graviton coherent state.

It was suggested in [16,25,26] that the backreaction from this radiation necessarily leads to a gradual loss of coherence and, subsequently, to a complete breakdown of the classical description. This happens after a so-called quantum break time, $t_{\rm Q}$.

The concept of quantum break time was originally introduced in [27] in the study of quantum evolution in a prototype many-body model invoked in [15] as a toy analog of a black hole N portrait [14]. It was shown [27] that in the regime in which the system possesses a Lyapunov exponent, λ, the quantum break time can be logarithmically short $t_{\rm Q} \sim \lambda^{-1} \ln(N)$, where N is the occupation number of constituents (in the present language, a "master mode"). The same system, in the classically stable regime exhibits a power-law break time, $t_{\rm Q} \propto \sqrt{N}$ [50].

The concept of quantum break time was applied to de Sitter in [16,25,26] and it was argued that for a cosmological constant source the quantum break time is bounded from above by $t_{\rm Q} \sim S_{\rm GH} R$. However, for a generic source, a shorter timescale, $t_{\rm Q} \sim R \ln(S_{\rm GH})$, emerges.

In recent years, other aspects of the phenomenon of quantum breaking have been studied extensively in various setups [26,106–116].

Now, based on the universality of the memory burden effect [1], it was argued in [22] that the phenomenon must be operative in de Sitter and must contribute into quantum breaking.

The idea of [22] is that de Sitter must posses memory modes which are responsible for initially degenerate microstates accounted by the Gibbons-Hawking entropy. It was concluded that, due to the depletion of the graviton coherent state via Gibbons-Hawking radiation [16,25,26], the memory burden effect must set in, latest, by the time $t_{\rm M} \sim S_{\rm GH} R$. This claim matches the previously suggested limit on quantum break time of de Sitter due to the loss of coherence and self-entanglement [16,25,26]. It is also very similar to the upper bound (107) on the memory burden time of a black hole. In general, the memory burden effect is one of the main engines of quantum breaking of de Sitter [22,24].

The observational signatures of the Hubble memory burden effect still remain to be understood. In inflationary context, it is expected to create departures from the standard semiclassical spectrum of density perturbations, with the amplitude increasing with the duration of inflation [22,24]. In this way, the memory burden effect provides a quantum clock that records the entire duration of the inflationary phase.

Although the analysis of the present paper was not directly intended at de Sitter, it nevertheless supports the

generic expected features previously proposed in [22,24]. This motivates future studies of applications of the memory burden effect to various cosmological backgrounds.

C. Memory burden in the Standard Model?

It was argued recently [8] that the Standard Model contains a saturon in form of a color glass condensate (CGC) [117]. This substance represents a saturated state of $N_{\rm glue} = 1/\alpha_{\rm s}(Q_{\rm s})$ gluons where $\alpha_{\rm s}(Q_{\rm s})$ is a running QCD coupling evaluated at a saturation scale $Q_{\rm s}$. As discussed in [8], CGC exhibits a striking correspondence with the black hole N portrait [14], with the gluons of CGC mapped on the graviton constituents of a black hole.

Being a saturated state, CGC is expected to be subjected to the memory burden effect, with potentially observable consequences. In particular, this can be manifested in emission of quanta by a factor of $\alpha_{\rm s}$ softer than the saturation scale $Q_{\rm s}$ [7].

ACKNOWLEDGMENTS

The work of G. D. was supported in part by the Humboldt Foundation under the Humboldt Professorship Award, by the European Research Council Gravities Horizon Grant AO No. 850 173-6, by the Deutsche Forschungsgemeinschaft (DFG, German Research Foundation) under Germany's Excellence Strategy—EXC-2111-390814868, Germany's Excellence Strategy under Excellence Cluster Origins EXC 2094-390783311. J. S. V. B. acknowledges the support from the Departament de Recerca i Universitats from Generalitat de Catalunya to the Grup de Recerca "Grup de Fisica Teorica UAB/IFAE" (Codi: 2021 SGR 00649) and the Spanish Ministry of Science and Innovation (Grant No. PID2020–115845 GB-I00/AEI/10.13039/501100011033). I. F. A. E. is partially funded by the CERCA program of the Generalitat de Catalunya. This study was supported by Ministerio de Ciencia e Innovacion with funding from European Union NextGenerationEU(PRTR-C17.I1) and by Generalitat de Catalunya. M. Z. acknowledges support by the National Natural Science Foundation of China (NSFC) through Grant No. 12350610240 "Astrophysical Axion Laboratories."

Funded by the European Union. Views and opinions expressed are however those of the authors only and do not necessarily reflect those of the European Union or European Research Council. Neither the European Union nor the granting authority can be held responsible for them.

[1] Gia Dvali, A microscopic model of holography: Survival by the burden of memory, arXiv:1810.02336.
[2] Jacob D. Bekenstein, Black holes and entropy, Phys. Rev. D **7**, 2333 (1973).
[3] Gia Dvali, Lukas Eisemann, Marco Michel, and Sebastian Zell, Black hole metamorphosis and stabilization by memory burden, Phys. Rev. D **102**, 103523 (2020).
[4] Gia Dvali, Entropy bound and unitarity of scattering amplitudes, J. High Energy Phys. 03 (2021) 126.
[5] Gia Dvali, Area law saturation of entropy bound from perturbative unitarity in renormalizable theories, Fortschr. Phys. **69**, 2000090 (2021).
[6] Gia Dvali, Unitarity entropy bound: Solitons and instantons, Fortschr. Phys. **69**, 2000091 (2021).
[7] Gia Dvali, Bounds on quantum information storage and retrieval, Phil. Trans. A. Math. Phys. Eng. Sci. **380**, 20210071 (2021).
[8] Gia Dvali and Raju Venugopalan, Classicalization and unitarization of wee partons in QCD and gravity: The CGC-black hole correspondence, Phys. Rev. D **105**, 056026 (2022).
[9] Gia Dvali and Otari Sakhelashvili, Black-hole-like saturons in Gross-Neveu, Phys. Rev. D **105**, 065014 (2022).
[10] Gia Dvali, Oleg Kaikov, and Juan Sebastián Valbuena-Bermúdez, How special are black holes? Correspondence with objects saturating unitarity bounds in generic theories, Phys. Rev. D **105**, 056013 (2022).
[11] Gia Dvali, Florian Kühnel, and Michael Zantedeschi, Vortices in black holes, Phys. Rev. Lett. **129**, 061302 (2022).
[12] Gia Dvali, Oleg Kaikov, Florian Kühnel, Juan Sebastian Valbuena-Bermúdez, and Michael Zantedeschi, Vortex effects in merging black holes and saturons, Phys. Rev. Lett. **132**, 151402 (2024).
[13] Juan Sebastián Valbuena-Bermúdez, The erasure of topological defects and the saturation phenomenon, Ph.D. thesis, Munich University, 2023.
[14] Gia Dvali and Cesar Gomez, Black hole's quantum N-portrait, Fortschr. Phys. **61**, 742 (2013).
[15] Gia Dvali and Cesar Gomez, Black holes as critical point of quantum phase transition, Eur. Phys. J. C **74**, 2752 (2014).
[16] Gia Dvali and Cesar Gomez, Quantum compositeness of gravity: Black holes, AdS and inflation, J. Cosmol. Astropart. Phys. 01 (2014) 023.
[17] Gia Dvali, Florian Kühnel, and Michael Zantedeschi, Primordial black holes from confinement, Phys. Rev. D **104**, 123507 (2021).
[18] Ana Alexandre, Gia Dvali, and Emmanouil Koutsangelas, New mass window for primordial black holes as dark matter from memory burden effect, Phys. Rev. D **110**, 036004 (2024).
[19] Valentin Thoss, Andreas Burkert, and Kazunori Kohri, Breakdown of Hawking evaporation opens new mass

window for primordial black holes as dark matter candidate, Mon. Not. R. Astron. Soc. **532**, 451 (2024).
[20] Shyam Balaji, Guillem Domènech, Gabriele Franciolini, Alexander Ganz, and Jan Tränkle, Probing modified Hawking evaporation with gravitational waves from the primordial black hole dominated universe, arXiv:2403.14309.
[21] Md Riajul Haque, Suvashis Maity, Debaprasad Maity, and Yann Mambrini, Quantum effects on the evaporation of PBHs: Contributions to dark matter, J. Cosmol. Astropart. Phys. 07 (2024) 002.
[22] Gia Dvali, Lukas Eisemann, Marco Michel, and Sebastian Zell, Universe's primordial quantum memories, J. Cosmol. Astropart. Phys. 03 (2019) 010.
[23] G. W. Gibbons and S. W. Hawking, Cosmological event horizons, thermodynamics, and particle creation, Phys. Rev. D **15**, 2738 (1977).
[24] Gia Dvali, Quantum gravity in species regime, arXiv:2103.15668.
[25] Gia Dvali and Cesar Gomez, Quantum exclusion of positive cosmological constant?, Ann. Phys. (Amsterdam) **528**, 68 (2016).
[26] Gia Dvali, Cesar Gomez, and Sebastian Zell, Quantum break-time of de Sitter, J. Cosmol. Astropart. Phys. 06 (2017) 028.
[27] Gia Dvali, Daniel Flassig, Cesar Gomez, Alexander Pritzel, and Nico Wintergerst, Scrambling in the black hole portrait, Phys. Rev. D **88**, 124041 (2013).
[28] Gia Dvali and Cesar Gomez, Black hole's 1/N hair, Phys. Lett. B **719**, 419 (2013).
[29] Gia Dvali, *S*-matrix and anomaly of de Sitter, Symmetry **13**, 3 (2020).
[30] https://youtu.be/boDpRXJnT5E
[31] See Supplemental Material at http://link.aps.org/supplemental/10.1103/PhysRevD.110.056029 for brief video summarizing the findings.
[32] Gia Dvali, Critically excited states with enhanced memory and pattern recognition capacities in quantum brain networks: Lesson from black holes, arXiv:1711.09079.
[33] Gia Dvali, Area law microstate entropy from criticality and spherical symmetry, Phys. Rev. D **97**, 105005 (2018).
[34] Gia Dvali, Black holes as brains: Neural networks with area law entropy, Fortschr. Phys. **66**, 1800007 (2018).
[35] Gia Dvali, Marco Michel, and Sebastian Zell, Finding critical states of enhanced memory capacity in attractive cold bosons, Eur. Phys. J. Quantum Technol. **6**, 1 (2019).
[36] Gia Dvali, Classicalization Clearly: Quantum transition into states of maximal memory storage capacity, arXiv:1804.06154.
[37] Gia Dvali, Cesar Gomez, Lukas Gruending, and Tehseen Rug, Towards a quantum theory of solitons, Nucl. Phys. **B901**, 338 (2015).
[38] T. D. Lee and G. C. Wick, Vacuum stability and vacuum excitation in a spin-0 field theory, Phys. Rev. D **9**, 2291 (1974).
[39] R. Friedberg, T. D. Lee, and A. Sirlin, A class of scalar-field soliton solutions in three space dimensions, Phys. Rev. D **13**, 2739 (1976).
[40] Sidney R. Coleman, Q-balls, Nucl. Phys. **B262**, 263 (1985); **B269**, 744(A) (1986).
[41] Alexander M. Safian, Sidney R. Coleman, and Minos Axenides, Some non-Abelian Q balls, Nucl. Phys. **B297**, 498 (1988).
[42] T. D. Lee and Y. Pang, Nontopological solitons, Phys. Rep. **221**, 251 (1992).
[43] Alexander Kusenko, Small Q balls, Phys. Lett. B **404**, 285 (1997).
[44] G. R. Dvali, A. Kusenko, and M. E. Shaposhnikov, New physics in a nutshell, or Q ball as a power plant, Phys. Lett. B **417**, 99 (1998).
[45] Alexander Kusenko and Mikhail E. Shaposhnikov, Supersymmetric Q balls as dark matter, Phys. Lett. B **418**, 46 (1998).
[46] A. Kusenko, M. E. Shaposhnikov, and P. G. Tinyakov, Sufficient conditions for the existence of Q balls in gauge theories, Pis'ma Zh. Eksp. Teor. Fiz. **67**, 229 (1998).
[47] Chan-ju Kim, Seyong Kim, and Yoon-bai Kim, Global nontopological vortices, Phys. Rev. D **47**, 5434 (1993).
[48] Mikhail S. Volkov and Erik Wohnert, Spinning Q balls, Phys. Rev. D **66**, 085003 (2002).
[49] Gia Dvali, Andre Franca, Cesar Gomez, and Nico Wintergerst, Nambu-Goldstone effective theory of information at quantum criticality, Phys. Rev. D **92**, 125002 (2015).
[50] Gia Dvali and Mischa Panchenko, Black hole type quantum computing in critical Bose-Einstein systems, arXiv:1507.08952.
[51] Artem Averin, Gia Dvali, Cesar Gomez, and Dieter Lust, Goldstone origin of black hole hair from supertranslations and criticality, Mod. Phys. Lett. A **31**, 1630045 (2016).
[52] Artem Averin, Gia Dvali, Cesar Gomez, and Dieter Lust, Gravitational black hole hair from event horizon supertranslations, J. High Energy Phys. 06 (2016) 088.
[53] S. W. Hawking, Particle creation by black holes, Commun. Math. Phys. **43**, 199 (1975); Commun. Math. Phys. **46**, 206(E) (1976).
[54] Gia Dvali, Black holes and large N species solution to the hierarchy problem, Fortschr. Phys. **58**, 528 (2010).
[55] Gia Dvali and Michele Redi, Black hole bound on the number of species and quantum gravity at LHC, Phys. Rev. D **77**, 045027 (2008).
[56] Gia Dvali, Nature of microscopic black holes and gravity in theories with particle species, Int. J. Mod. Phys. A **25**, 602 (2010).
[57] Gia Dvali and Cesar Gomez, Quantum information and gravity cutoff in theories with species, Phys. Lett. B **674**, 303 (2009).
[58] Gia Dvali and Dieter Lust, Evaporation of microscopic black holes in string theory and the bound on species, Fortschr. Phys. **58**, 505 (2010).
[59] Gia Dvali and Cesar Gomez, Species and strings, arXiv:1004.3744.
[60] Remo Ruffini and John A. Wheeler, Introducing the black hole, Phys. Today **24**, No. 1, 30 (1971).
[61] Jacob D. Bekenstein, Transcendence of the law of baryon-number conservation in black-hole physics, Phys. Rev. Lett. **28**, 452 (1972).
[62] C. Teitelboim, Nonmeasurability of the baryon number of a black-hole, Lett. Nuovo Cimento **3S2**, 326 (1972).
[63] Hugh Luckock and Ian Moss, Black holes have skyrmion hair, Phys. Lett. B **176**, 341 (1986).

[64] P. Bizon and T. Chmaj, Gravitating skyrmions, Phys. Lett. B **297**, 55 (1992).
[65] Serge Droz, Markus Heusler, and Norbert Straumann, New black hole solutions with hair, Phys. Lett. B **268**, 371 (1991).
[66] Gia Dvali and Alexander Gußmann, Aharonov–Bohm protection of black hole's baryon/skyrmion hair, Phys. Lett. B **768**, 274 (2017).
[67] Gia Dvali and Alexander Gußmann, Skyrmion black hole hair: Conservation of baryon number by black holes and observable manifestations, Nucl. Phys. **B913**, 1001 (2016).
[68] Lawrence M. Krauss and Frank Wilczek, Discrete gauge symmetry in continuum theories, Phys. Rev. Lett. **62**, 1221 (1989).
[69] John Preskill and Lawrence M. Krauss, Local discrete symmetry and quantum mechanical hair, Nucl. Phys. **B341**, 50 (1990).
[70] Gia Dvali and Lukas Eisemann, Perturbative understanding of nonperturbative processes and quantumization versus classicalization, Phys. Rev. D **106**, 125019 (2022).
[71] G. Dvali, C. Gomez, R. S. Isermann, D. Lüst, and S. Stieberger, Black hole formation and classicalization in ultra-Planckian $2 \to N$ scattering, Nucl. Phys. **B893**, 187 (2015).
[72] Andrea Addazi, Massimo Bianchi, and Gabriele Veneziano, Glimpses of black hole formation/evaporation in highly inelastic, ultra-Planckian string collisions, J. High Energy Phys. 02 (2017) 111.
[73] Lowell S. Brown, Summing tree graphs at threshold, Phys. Rev. D **46**, R4125 (1992).
[74] E. N. Argyres, Ronald H. P. Kleiss, and Costas G. Papadopoulos, Amplitude estimates for multi—Higgs production at high-energies, Nucl. Phys. **B391**, 42 (1993).
[75] M. B. Voloshin, Estimate of the onset of nonperturbative particle production at high-energy in a scalar theory, Phys. Lett. B **293**, 389 (1992).
[76] A. S. Gorsky and M. B. Voloshin, Nonperturbative production of multiboson states and quantum bubbles, Phys. Rev. D **48**, 3843 (1993).
[77] M. V. Libanov, V. A. Rubakov, D. T. Son, and Sergey V. Troitsky, Exponentiation of multiparticle amplitudes in scalar theories, Phys. Rev. D **50**, 7553 (1994).
[78] M. V. Libanov, D. T. Son, and Sergey V. Troitsky, Exponentiation of multiparticle amplitudes in scalar theories. 2. Universality of the exponent, Phys. Rev. D **52**, 3679 (1995).
[79] D. T. Son, Semiclassical approach for multiparticle production in scalar theories, Nucl. Phys. **B477**, 378 (1996).
[80] A. Monin, Inconsistencies of higgsplosion, arXiv:1808.05810.
[81] Burkhard Kleihaus, Jutta Kunz, and Meike List, Rotating boson stars and Q-balls, Phys. Rev. D **72**, 064002 (2005).
[82] Gia Dvali, Hui Liu, Oleg Kaikov, and Juan Sebastián Valbuena-Bermúdez (to be published).
[83] R. L. Davis and E. P. S. Shellard, Cosmic vortons, Nucl. Phys. **B323**, 209 (1989).
[84] Jose A. de Freitas Pacheco, Elias Kiritsis, Matteo Lucca, and Joseph Silk, Quasiextremal primordial black holes are a viable dark matter candidate, Phys. Rev. D **107**, 123525 (2023).
[85] Nima Arkani-Hamed, Savas Dimopoulos, and G. R. Dvali, The hierarchy problem and new dimensions at a millimeter, Phys. Lett. B **429**, 263 (1998).
[86] Luis A. Anchordoqui, Ignatios Antoniadis, and Dieter Lust, More on black holes perceiving the dark dimension, Phys. Rev. D **110**, 015004 (2024).
[87] Luis A. Anchordoqui, Ignatios Antoniadis, and Dieter Lust, Dark dimension, the swampland, and the dark matter fraction composed of primordial black holes, Phys. Rev. D **106**, 086001 (2022).
[88] Paul M. Saffin, Qi-Xin Xie, and Shuang-Yong Zhou, Q-ball superradiance, Phys. Rev. Lett. **131**, 111601 (2023).
[89] Michael Zantedeschi, On structure and primordial origin of black holes, Ph.D. thesis, Munich University, 2022.
[90] Don N. Page, Particle emission rates from a black hole. 2. Massless particles from a rotating hole, Phys. Rev. D **14**, 3260 (1976).
[91] https://www.youtube.com/watch?v=t29WUvZM-io&ab_channel=MichaelZantedeschi
[92] https://www.youtube.com/watch?v=zorkQSYCliU&t=0s&ab_channel=MichaelZantedeschi
[93] Richard Battye and Paul Sutcliffe, Q-ball dynamics, Nucl. Phys. **B590**, 329 (2000).
[94] Michael P. Kinach and Matthew W. Choptuik, Dynamical evolution of $U(1)$ gauged Q-balls in axisymmetry, Phys. Rev. D **107**, 035022 (2023).
[95] Ya. B. Zel'dovich and I. D. Novikov, The hypothesis of cores retarded during expansion and the hot cosmological model, Sov. Astron. **10**, 602 (1967).
[96] Stephen Hawking, Gravitationally collapsed objects of very low mass, Mon. Not. R. Astron. Soc. **152**, 75 (1971).
[97] Bernard J. Carr and S. W. Hawking, Black holes in the early Universe, Mon. Not. R. Astron. Soc. **168**, 399 (1974).
[98] G. F. Chapline, Cosmological effects of primordial black holes, Nature (London) **253**, 251 (1975).
[99] Bernard Carr, Florian Kuhnel, and Marit Sandstad, Primordial black holes as dark matter, Phys. Rev. D **94**, 083504 (2016).
[100] Antonio Riotto and Joe Silk, The future of primordial black holes: Open questions and roadmap, arXiv:2403.02907.
[101] B. J. Carr, Kazunori Kohri, Yuuiti Sendouda, and Jun'ichi Yokoyama, New cosmological constraints on primordial black holes, Phys. Rev. D **81**, 104019 (2010).
[102] Jérémy Auffinger, Primordial black hole constraints with Hawking radiation—A review, Prog. Part. Nucl. Phys. **131**, 104040 (2023).
[103] Gia Dvali, Juan Sebastián Valbuena-Bermúdez, and Michael Zantedeschi, Dynamics of confined monopoles and similarities with confined quarks, Phys. Rev. D **107**, 076003 (2023).
[104] Gia Dvali, Saturon dark matter, arXiv:2302.08353.
[105] Lasha Berezhiani, Gia Dvali, and Otari Sakhelashvili, de Sitter space as a BRST invariant coherent state of gravitons, Phys. Rev. D **105**, 025022 (2022).
[106] Gia Dvali and Cesar Gomez, Black hole's information group, arXiv:1307.7630.
[107] Lasha Berezhiani, On corpuscular theory of inflation, Eur. Phys. J. C **77**, 106 (2017).

[108] Tanmay Vachaspati, Quantum backreaction on classical dynamics, Phys. Rev. D **95**, 125002 (2017).
[109] Gia Dvali and Sebastian Zell, Classicality and quantum break-time for cosmic axions, J. Cosmol. Astropart. Phys. 07 (2018) 064.
[110] A. Kovtun and M. Zantedeschi, Breaking BEC, J. High Energy Phys. 07 (2020) 212.
[111] A. Kovtun and M. Zantedeschi, Breaking BEC: Quantum evolution of unstable condensates, Phys. Rev. D **105**, 085019 (2022).
[112] Lasha Berezhiani and Michael Zantedeschi, Evolution of coherent states as quantum counterpart of classical dynamics, Phys. Rev. D **104**, 085007 (2021).
[113] Lasha Berezhiani, Giordano Cintia, and Michael Zantedeschi, Background-field method and initial-time singularity for coherent states, Phys. Rev. D **105**, 045003 (2022).
[114] Oleg Kaikov, Fast prescramblers, Phys. Rev. D **107**, 116008 (2023).
[115] Marco Michel and Sebastian Zell, The timescales of quantum breaking, Fortschr. Phys. **71**, 2300163 (2023).
[116] Lasha Berezhiani, Giordano Cintia, and Michael Zantedeschi, Perturbative construction of coherent states, Phys. Rev. D **109**, 085018 (2024).
[117] Francois Gelis, Edmond Iancu, Jamal Jalilian-Marian, and Raju Venugopalan, The color glass condensate, Annu. Rev. Nucl. Part. Sci. **60**, 463 (2010).